Accepted Article

MAVEN case studies of plasma dynamics in low altitude crustal magnetic field at Mars 1: Dayside ion spikes associated with radial crustal magnetic fields

Y. I. J. Soobiah[1,2*], Jared R. Espley[1], John E. P. Connerney[1], Jacob R. Gruesbeck[1], Gina A. DiBraccio[1], Jasper Halekas[3], Laila Andersson[4], Christopher M. Fowler[4], Robert J. Lillis[5], David L. Mitchell[5], Christian Mazelle[6], Yuki Harada[7], Takuya Hara[5], Glyn Collinson[1,8], David Brain[4], Shaosui Xu[5], Shannon M. Curry[5], James P. McFadden[5], Mehdi Benna[1] and Bruce M. Jakosky[4].

[1]Solar System Exploration Division, NASA Goddard Space Flight Center, Greenbelt, USA.

[2]Department of Astronomy, University of Maryland, College Park, Maryland, USA.

[3]Department of Physics and Astronomy, University of Iowa, Iowa City, USA.

[4]Laboratory for Atmospheric and Space Physics (LASP), University of Colorado, Boulder, USA.

[5]Space Sciences Laboratory (SSL), University of California, Berkeley, USA.

[6]IRAP, University of Toulouse, CNRS, UPS, CNES, Toulouse, France.

[7]Department of Geophysics, Kyoto University, Japan.

[8]Institute for Astrophysics and Computational Sciences, Catholic University of America, Washington, District of Columbia, USA.

Key Points:

- Investigated plasma transport and associated electrodynamics during ion energy flux spikes in radial crustal magnetic field on the Mars dayside.
- Precipitating ion and electron energy flux spikes on closed field consisting of ion beams E>1.4 keV and broad ion distributions E<1.4 keV.
- Considered impact of low altitude precipitating O^+ ions E>25 eV on localized heating and atmospheric escape.

This article has been accepted for publication and undergone full peer review but has not been through the copyediting, typesetting, pagination and proofreading process which may lead to differences between this version and the Version of Record. Please cite this article as doi: 10.1029/2018JA025569

*Current address, NASA/GSFC, Code 695, Greenbelt, MD 20770, USA.

Corresponding author: Y. I. J. Soobiah, yasir.i.soobiah@nasa.gov

©2018 American Geophysical Union. All rights reserved.

Accepted Article

Abstract

We report for the first time, simultaneous ion, electron, magnetic field vector and electric field wave measurements made possible by MAVEN, during ion energy flux spikes in low altitude radial crustal magnetic fields on the Mars dayside. Observations show energetic electrons and ions (E>25 eV) precipitating on magnetic field lines assumed as closed. Ions (E<1.4 keV) display broad velocity distributions towards Mars, showing ions flowing from higher altitude possibly after magnetic reconnection or loss cone filling from pitch angle scattering effects. Precipitating ions (E<1.4 keV) show non-adiabatic features depending on ion mass and energy and returning ions (E<1.4 keV) show evidence of conserving the first adiabatic invariant in a mirror field. We observe magnetic field perturbations up to 60 nT, electric field wave amplitudes up to 38 mV/m and brief periods of peaked electron spectra. At ~175 km and at times MAVEN is below the mirroring altitude of electrons, we observe mirroring and transverse heating of H^+ ions alongside increased electric field wave amplitude fluctuations. It suggests field aligned potential drops result from different mirror altitudes of ions and electrons. Ions E>1.4 keV (O^+) occur as injected accelerated ion beams and ions heated after energization or deceleration. Energy dispersed keV ions suggest a selection effect in radial magnetic fields for lower energy Marsward ions, compared to reflection of higher energy anti-Sunward ions. Precipitating keV ions show energy deposition rates of 3.6×10^{-6} W/m^2 and sputtering escape rates from precipitating O^+ ions of 1.5×10^5 /(cm^2.sec) and 2.1×10^6 /(cm^2.sec) are calculated.

1 Introduction

Until the arrival of the Mars Atmosphere and Volatile Evolution (MAVEN) [*Jakosky et al.*, 2015] mission at Mars on September 22nd, 2014, it had not been possible to achieve a complete understanding of the plasma transport processes and associated electrodynamics effects in low altitude (<300 km) regions of the Martian crustal magnetic fields. This is the case since previous Mars missions either did not reach such regions or could not make the simultaneous ion, electron, magnetic field vector and electric field wave measurements performed by MAVEN's Particle and Fields Package (PFP). Of particular importance to this goal is being able to characterize the kinetic behavior of ions from ion velocity distributions formed with use of in-situ vector measurements of the magnetic field, which has not been achieved before in the low altitude crustal magnetic fields of Mars. Characterizing the behavior of ions is crucial for understanding the plasma dynam-

©2018 American Geophysical Union. All rights reserved.

Accepted Article

ics of planetary magnetospheres since ions make the dominant contribution to the transport and loss of mass within a magnetosphere and cases of ion precipitation onto an ionosphere/atmosphere can represent times of large kinetic energy transfer when colliding with the atmosphere [*Fang et al.*, 2013].

As a planet without a strong magnetic field of internal origin, but with a thin tenuous atmosphere, Mars interaction with the solar wind typically follows that of an unmagnetized atmospheric obstacle to the solar wind [*Nagy et al.*, 2004; *Vaisberg*, 2015]. As such the solar wind magnetic field and plasma passing over the Martian obstacle forms an induced magnetosphere through mass loading of the solar wind magnetic field with planetary plasma and the induction of currents and magnetic fields in the Martian ionosphere. An induced magnetosphere involves numerous processes that can energize ions [*Dubinin et al.*, 2011], the most prominent of which include ion pick up from the acceleration of exospheric ions by the solar wind convective electric field [*Dubinin et al.*, 2006b; *Yamauchi et al.*, 2006, 2008; *Rahmati et al.*, 2015], plasma sheet acceleration from the j×B force due to magnetic shear stresses in the magnetotail [*Dubinin et al.*, 1993] and the day-to-night flow of ionospheric plasma associated with the day-to-night pressure gradient [*Knudsen et al.*, 1981; *Fränz et al.*, 2010]. Another potential source of energetic ions at Mars is the ionized hot hydrogen and oxygen corona, simulations of which results in O^+ ions with E>1 keV close to Mars [*Kallio et al.*, 2008]. The gyroradius of these energetic ion populations can vary between hundreds of km (heavy ions with E<1 keV and protons with E~1 keV) to multiples of the Martian radii (heavy ions with E>10 keV) and results in ions that are mostly unmagnetized.

Mars is also host to strong localized crustal sources of magnetic field [*Acuña et al.*, 1998; *Connerney et al.*, 2001, 2005] that are expected to produce local perturbations in the interaction of the solar wind with Mars over the planetary scale, leading to a time and spatial variable obstacle to the solar wind [*Brain et al.*, 2005]. The way in which these pockets of strongly magnetized crust modify plasma dynamics of the induced magnetosphere is still poorly understood in terms of in-situ particle and fields observations and also how the processes involved, enhance or inhibit atmospheric escape at Mars. Regions of the crustal magnetic field have been observed by previous Mars missions, Mars Global Surveyor (MGS) and Mars Express (MEX), to host magnetic field and particles signatures indicative of different magnetospheric processes that accelerate / energize particles and contribute to the escape of the Martian atmosphere. Signatures of magnetic flux ropes

©2018 American Geophysical Union. All rights reserved.

Accepted Article

have been identified in a number of different regions around Mars [*Briggs et al.*, 2012]. Some magnetic flux rope observations have been related to magnetic reconnection between magnetic fields from the solar wind and crustal magnetic fields [*Brain et al.*, 2010; *Soobiah et al.*, 2014; *Hara et al.*, 2017a], as well as the detachment of crustal magnetic fields and a bulk escape of the atmospheric plasma of Mars [*Brain et al.*, 2010].

Localized intensifications of electron energy flux, also referred to as electron spikes, that correlate with cusp regions of the crustal magnetic fields have been associated with regions of open magnetic field and the precipitation of magnetosheath electrons towards Mars, made possible by magnetic reconnection between solar wind and crustal magnetic fields [*Mitchell et al.*, 2001; *Soobiah et al.*, 2006; *Halekas et al.*, 2008]. This compares to observations on large spatial scales that show a greater probability of lower electron fluxes for regions of higher crustal magnetic field strength [*Fränz et al.*, 2006]. Electron spikes and localized enhancements in the peak ionospheric electron density have also been observed in the vicinity of cusps of the crustal magnetic fields on the dayside of Mars as associated with plasma heating from the convection of ionospheric plasma rather than from the precipitation of magnetosheath / solar wind electrons [*Nielsen et al.*, 2007]. Here, convection of ionospheric plasma, driven by electric fields induced at the interface between the crustal magnetic fields and the solar wind flow, heats the plasma of the low altitude crustal magnetic field cusps, which can relate to a reduction in the electron-ion recombination rate that in-turn increases the equilibrium electron density [*Nielsen et al.*, 2007].

Observations of auroral emission in regions of the Martian crustal magnetic field [*Bertaux et al.*, 2005] are indicative of processes taking place at Mars that are analogous to the auroral processes of plasma acceleration and energization at Earth [*Lundin et al.*, 2006b]. Indeed, this is supported by the strong correlation of crustal magnetic field regions with observations in the high altitude nightside of Mars of "inverted-V" electron and ion energy-time structures showing the acceleration of electrons towards Mars and the acceleration of ions away from Mars [*Lundin et al.*, 2006a; *Gérard et al.*, 2015], Moreover, peaked electron energy distributions have been observed on the circular mapping orbits of MGS at 400 km altitude to correlate with regions most likely to involve open magnetic field on the nightside of Mars [*Brain et al.*, 2006]. Such examples of accelerated electrons are considered as evidence for the auroral acceleration in a quasi-static electric potential drop at Mars [*Lundin et al.*, 2006a,b; *Brain et al.*, 2006]. In addition, at the times of peaked electron distributions, MGS also observed perturbations in the magnetic

©2018 American Geophysical Union. All rights reserved.

Accepted Article

field indicative of a deflection in the magnetic field from field aligned currents [*Brain et al.*, 2006; *Halekas et al.*, 2008]. Also, calculations using MGS pre-mapping orbit data show enhanced Hall conductivity in regions of crustal magnetic fields between 100 km - 250 km and greater likelihood of perpendicular currents being supported in these regions [*Opgenoorth et al.*, 2010]. Such properties are typical of auroral phenomena and solar wind ionosphere coupling at Earth that support the presence of parallel electric fields and potential drops. The theory of such structures at Earth has been shown to also be applicable to Mars [*Dubinin et al.*, 2008]. Furthermore, recent analysis of MGS electron pitch angle data has shown evidence of field-aligned electrostatic potentials in the Martian ionosphere, which possibly form due to electric currents associated with solar wind ionosphere coupling in regions of crustal magnetic field [*Lillis et al.*, 2018]. The particle precipitation and associated field aligned electric fields related to nightside aurora or dayside coupling between the solar wind and the Martian ionosphere, has the potential to affect the dynamics of the Martian ionosphere and the neutral atmosphere, leading to an outflow of ions [*Ergun et al.*, 2006].

While previous observations at Mars have been able to characterize in detail the properties of electron and magnetic field signatures in regions of the crustal magnetic field, a similar level of detail in the properties of ion signatures and their relation to the plasma dynamics of the Martian crustal magnetic fields is still limited. Previous studies by MEX have shown a poor one to one correlation between electron precipitation signatures and corresponding ion signatures, where the general low energy / cold component of heavy-ions flowing away from Mars remain mostly unchanged [*Soobiah et al.*, 2013]. This was considered the result of the finite gyroradius effect from the large gyroradius of heavy-ions in regions of crustal magnetic field. Cases of precipitating energetic electrons in crustal magnetic field cusps have been associated with the auroral-like outflow of planetary ions [*Dubinin et al.*, 2009], as well as the simultaneous presence of cold ionospheric ions and a more energetic component of heated ions [*Dubinin et al.*, 2011].

Statistical studies using MEX data have shown how crustal magnetic field regions can effect ion dynamics to either inhibit ion escape rates [*Lundin et al.*, 2011; *Nilsson et al.*, 2011] or result in enhanced escape rates for pre-terminator locations between 60° - 80° solar zenith angles (SZA) [*Ramstad et al.*, 2016]. Modeling of the solar wind interaction with Mars arrive at similar results where ion escape rates are shown to respond to the presence of crustal magnetic fields, where the crustal fields can act as a protective shield

©2018 American Geophysical Union. All rights reserved.

Accepted Article

deflecting the solar wind around the Martian atmosphere [*Fang et al.*, 2010; *Dong et al.*, 2015] or when placed close to dawn or dusk local times cause increased escape rates [*Ma et al.*, 2014; *Fang et al.*, 2015]. Furthermore, regions of crustal magnetic field may drive the precipitation of pick-up ions towards the atmosphere of Mars, leading to an increase in energy deposition and also sputtering [*Li et al.*, 2011; *Curry et al.*, 2015], a process thought to be important in the escape of the Martian atmosphere [*Leblanc and Johnson*, 2001, 2002].

In this paper, using data from the MAVEN spacecraft, we examine for the first time at Mars the kinetic properties of ion transport and the associated plasma dynamics observed during broad energy range spikes of ion energy flux in low altitude regions of radial crustal magnetic field on the dayside of Mars. The case studies reported here include the first observations made in the low altitude crustal magnetic field regions of Mars of rare and extraordinary ion energy-time structures made up of ion spikes that extend to keV energies when coinciding with energy dispersed structures of keV ions that develop into energy-time structures of keV ion bands. This work also accompanies the companion study by *Hara et al.* [2018] showing statistical evidence for the crustal magnetic field control of precipitating ion fluxes observed by MAVEN into the upper atmosphere of Mars.

2 Dataset

This study presents data from the PFP suite of instruments on MAVEN. The Solar Wind Ion Analyzer (SWIA) [*Halekas et al.*, 2015a] and the SupraThermal And Thermal Ion Composition (STATIC) [*McFadden et al.*, 2015] provides measurements of ion energy distributions, with STATIC providing ion mass information. The Solar Wind Electron Analyzer (SWEA) [*Mitchell et al.*, 2016] provides measurements of the electron energy distributions at high time cadence of 2 s. Note, units of energy flux or 'EFlux' presented here using SWIA, STATIC and SWEA data corresponds to units of eV/(cm^2·sec·sr·eV). The MAGnetic field investigation (MAG) [*Connerney et al.*, 2015a,b] provides three-dimensional magnetic field measurements with a maximum cadence of 32 vector samples per second. The MAG vector is presented in the planetocentric reference frame where positive B_ϕ is the component of magnetic field directed Eastward, positive B_θ is the component of magnetic field directed Southwards and positive B_r is the component of magnetic field directed radially away from the planet. The Langmuir Probe and Waves (LPW) instrument

©2018 American Geophysical Union. All rights reserved.

Accepted Article

[*Andersson et al.*, 2015] is used to provide single component electric field measurements from DC to ~2 MHz.

3 The coincidence of broad energy range ion spikes and keV ion band features in low altitude radial crustal magnetic field

3.1 MAVEN observations from October 26th, 2015

Fig. 1 shows MAVEN PFP data from orbit 2088 on October 26th, 2015 as MAVEN moved outbound from periapsis over a region of strong crustal magnetic field, revealing extraordinary ion energy-time structures in low altitude (>300 km) crustal magnetic fields on the dayside of Mars. That is the localized broad energy range spikes in ion energy flux in regions of radial crustal magnetic field that also coincide with the energy dispersion of keV ions and a energy-time keV ion band feature. Between times of 10:47:20 UT - 10:47:32 UT and 10:50:44 UT - 10:51:00 UT SWIA observes prominent spikes in ion energy flux over a broad range in energy, between 25 eV - ~1 keV. The ion spikes, referred to hereafter as ion spike 1 and 2, occur as temporally and spatially confined structures in regions of increased radial magnetic field and coincide with a change in sign of one of the horizontal components of magnetic field.

As observed by SWIA is a band of ions in the energy-time spectrogram between 1.4 keV - 10 keV and 10:50:00 UT - 10:54:28 UT. Close to ion spike 2 between 10:51:0 UT - 10:51:52 UT, ions from the keV ion band are observed below 4 keV and to increase in energy such that between 10:51:52 UT - 10:54:28 UT the keV ion band is observed between 4 keV - 10 keV. STATIC observations (cf. Fig. 1(b)-(d)) show the keV ion band is formed of O^+ ions. The origin of such ions are unknown, but similar observations of keV ions from the induced magnetosphere of Mars have been associated with O^+ ions picked-up by the solar wind that are precipitating towards Mars in the -E hemisphere [*Hara et al.*, 2017b]. A more detailed investigation of the properties of this keV ions band feature is left for future work.

STATIC observations (cf. Fig. 1(b)-(d)) show ion spike 1 and 2 composed of multiple ion populations, O^+ and O_2^+ ions from 25 eV - 0.1 keV characteristic of planetary ions, H^+ ions from 0.1 keV - ~1 keV characteristic of the magnetosheath ions. Ion spike 2 also includes O^+ ions with energies >1 keV, characteristic of the O^+ ions picked-up by the solar wind. Beyond 10:54:00 UT as the altitude of MAVEN increases and strength of

©2018 American Geophysical Union. All rights reserved.

Accepted Article

the crustal magnetic field decreases, there is an extended region of ions between 25 eV - 10 keV with low energy flux showing a similar make up of ions observed during ion spike 1 and 2.

Fig. 1(f) and (g) shows during ion spike 1 and 2 lower and medium energy ion populations are characterized by distributions of the angle of flow to Mars depending on energy that are broad and asymmetric, with a greater energy flux of ions observed in the hemisphere directed towards Mars. Fig. 1(e) shows the higher energy ion population during ion spike 1 and 2 have ion energy distributions are far narrower in angular range, that is more field aligned and directed towards Mars compared to the lower and medium energy ion populations.

SWEA measures a slight enhancement in the energy flux of electrons at energies >60 eV (cf. Fig. 1(h)) neighboring ion spike 2, between 10:51:03 UT - 10:51:05 UT, referred to hereafter as electron spike A (labeled to the left of the electron spike). Fig. 1(i) shows the modest electron spike has electron pitch angles that are mostly anti-parallel to the magnetic field and directed towards Mars. Throughout most of the time period of Fig. 1, including the duration of ion spikes 1 and 2 and electron spike A, field aligned photoelectrons are observed directed both toward and away from Mars (not shown). The topology of magnetic field related to such observations is discussed in section 4.

Fig. 1(k) shows how both ion spike 1 and 2 coincide with periods of large perturbations in the magnetic field vectors from the background magnetic field, with the perturbation in the magnetic field showing typical magnitudes of ±10 nT. Note, an approximate background magnetic field is obtained by the addition of the background magnetic field from Mars, assumed as that from the *Morschhauser et al.* [2014] crustal magnetic field model, and a background magnetic field from external sources. The background magnetic field from external sources is determined by subtracting the *Morschhauser et al.* [2014] crustal magnetic field model from the MAG measured magnetic field and then using a low-pass filter with a 0.5 Hz (20 s) cut-off frequency on the difference. This method leads to a more desirable midline fit across magnetic field perturbations for the variety of cases investigated here as compared to the removal of a low-pass filter with a 0.5 Hz (20 s) cut-off frequency of the total magnetic field alone.

The black axis and data points of Fig. 1(l) shows how both ion spike 1 and 2 coincide with periods of increased electric field wave amplitude, with typical values around

©2018 American Geophysical Union. All rights reserved.

Accepted Article

±2 mV/m. Note, the electric field wave amplitude has been obtained using a sliding window average of the raw electric field data taken from spectra of plasma wave electric field recorded during LPW's passive and active modes (see *Andersson et al.* [2015] for details on LPW operation). Fig. 1(l) has also accounted for low frequency noise from LPW as described in *Fowler et al.* [2017]. Near the onset of ion spike 1, around 10:47:21 UT, there are large outliers for both the magnetic field perturbation of ~36 nT and electric field wave amplitude that fluctuates between ±40 mV/m as shown by the red axis and symbols. These large electric fields were observed with a stable background electric field and did not result from the sudden change in the background electric field typified when crossing sharp plasma boundaries [*Fowler et al.*, 2017]. In order to determine an electric field, the LPW booms are separated by 12.68 m in the direction parallel to the Y-axis of the MAVEN spacecraft frame. The angle of this direction from the local magnetic field is given by the light blue line in Fig. 1(l) with the accompanying axis to the right of the panel. This shows during the times of ion spikes 1 and 2, the increased electric field wave amplitude measured by LPW corresponds to electric fields perpendicular or oblique to the magnetic field.

©2018 American Geophysical Union. All rights reserved.

Accepted Article

3.2 MAVEN observations from June 2nd, 2015

Fig. 2 shows MAVEN PFP data from orbit 1307 on June 2nd, 2015 as MAVEN passed periapsis over a region of strong to moderate crustal magnetic field. As with observations presented in Fig. 1(a) from orbit 2088 of MAVEN, Fig. 2(a) shows SWIA observes spikes in ion energy flux between 25 eV - ~1 keV between times of 06:08:42 UT - 06:08:59 UT, 06:10:58 UT - 06:11:18 UT, 06:13:18 UT - 06:14:02 UT and 06:14:50 UT - 06:15:46 UT. The ion spikes, referred to hereafter as ion spikes 3, 4, 5 and 6 , are temporally and spatially confined to regions of increased strength in the radial magnetic field and coincide with a change in sign of one of the horizontal components of magnetic field.

For completeness STATIC data is included in Fig. 2(b)-(c), and show STATIC measurements affected by background noise as well as a change in the operating mode of the instrument. Prior to 06:11:36 UT and adjacent to periapsis, STATIC is in conic mode and measures ions between 0.1 eV - 500 eV. After 06:11:42 UT and during periapsis, STATIC is in ram mode and measures ions between 0.1 eV - 50 eV [*McFadden et al.*, 2015]. Note, between 06:08:30 UT - 06:08:54 UT, STATIC is able to distinguish an energization of O_2^+ ions during ion spike 3 (cf. Fig. 2(d)).

Fig. 2(a) shows a band of ions between energies 5 keV - 14 keV observed by SWIA between 06:09:30 UT - 06:13:31 UT. This is comparable to the ion band feature presented in Fig. 1(a) and also displays a cut-off in time with the appearance of ion spike 5. The similarity in appearance and energies of this ion band feature to that observed in Fig. 1(a) and (c) would suggest the ion band feature of Fig. 2(a) is the result of O^+ ions. An additional band of ions observed between 0.7 keV - 1.4 keV (peaking at ~1 keV) follows features identified as penetrating solar wind H^+ ions in the Martian ionosphere [*Halekas et al.*, 2015b].

Fig. 2(f)-(g) shows that the lower energy ion population during ion spike 3 and 4 and the lower and medium energy ion populations during ion spike 5 and 6 are characterized by broad energy distributions that are asymmetric with greater energy flux of ions directed towards Mars. During ion spike 4, 5 and 6, there is also an appreciable component of ions moving away from Mars. Fig. 2(e) shows the higher energy ion population during ion spike 5 displays an increase in the field aligned component of ions directed towards Mars. Whereas the high energy ion distributions in surrounding regions are dominated by ions moving anti-Sunward (broad angular distribution at larger angles to Mars).

©2018 American Geophysical Union. All rights reserved.

Accepted Article

Accompanying ion spike 3, 5 and 6, between 06:08:33 UT - 06:08:59 UT, 06:13:21 UT - 06:13:35 UT, 06:14:55 UT - 06:15:01 UT and 06:15:19 UT - 06:15:29 UT, SWEA measures appreciable spikes in the energy flux of electrons over a few hundreds of eV (cf. Fig. 2(h)). The electron spikes from Fig. 2(h) are referred to hereafter as electron spikes B, C, D and E electron spikes (as labeled to the left of each electron spike).

Fig. 2(i) shows the pitch angle distributions of the electron spikes are formed of field aligned electrons directed towards Mars. Note, electron spike B, C and E occur with a sharp drop off in the normalized energy flux in the hemisphere directed away from Mars, at angles from around 60° for electron spike B and from around 90° for electron spikes C and E respectively.

At the time of the ion spikes, Fig. 2(k) and (l) shows perturbations in the magnetic field vectors from the background magnetic field, typically around ±10 nT in magnitude, as well as increased electric field wave amplitude, varying between ±2 mV/m (black axis and data points) - ±20 mV/m (red axis and data points). Note, ion spike 3 and 4 occur with large deflections in magnetic field of up to 60 nT magnitude. As part of the electric field wave amplitude measured by LPW, but not shown are outliers of ~70 mV/m at 06:11:47 UT, ~63 mV/m at 06:12:07 UT and ~100 mV/m at 06:15:00 UT, associated with sudden changes in the background electric field typified when crossing sharp plasma boundaries [*Fowler et al.*, 2017]. As in the previous case, the angle the Y-axis of the MAVEN spacecraft frame makes with the local magnetic field (light blue line and axis) shows that during the times of ion spikes 3 to 6, the increased electric field wave amplitude measured by LPW corresponds to electric fields perpendicular or oblique to the magnetic field.

4 Electron spikes in low altitude radial crustal magnetic field that are open or closed.

Different methods are available to derive magnetic field topology at Mars from electron measurements using electron pitch angle distributions [*Brain et al.*, 2007] or pitch angle resolved electron energy spectra [*Xu et al.*, 2017]. For the former method, regions of closed magnetic field are identified by two-sided loss cones (trapped distributions - both dayside and nightside), fully isotropic distributions (dayside) and plasma void distributions (nightside). Open magnetic field are identified in regions of strong crustal magnetic field where the field-aligned electrons returning from the planet is much reduced compared to

©2018 American Geophysical Union. All rights reserved.

Accepted Article

other pitch angles, that is one-sided loss cones [*Brain et al.*, 2007]. The type of electron energy spectra measured serves as an indication of the connection a magnetic field line has with certain regions of plasma. For example closed magnetic fields will have both ends of the magnetic field connected to the source region of the ionosphere and would show photoelectrons traveling in both directions along the magnetic field [*Xu et al.*, 2017]. Open magnetic field lines would have one end connected to the source region of the ionosphere and one end connected to the solar wind / magnetosheath and would show photoelectrons traveling away from Mars and solar wind / magnetosheath electrons traveling towards Mars [*Xu et al.*, 2017]. Draped magnetic field lines would have both ends connected the solar wind / magnetosheath and would show solar wind / magnetosheath electrons traveling in both directions along the magnetic field [*Dubinin et al.*, 1994; *Xu et al.*, 2017].

Electron loss cones indicative of open magnetic field topology are observed in cases of electron spike A for energies >70 eV (not shown) and electron spike B as shown by the average electron pitch angle distribution between 50 eV - 100 eV (cf. Fig. 2(i)). Note, for energies <70 eV, electron spike A has a more bi-directional electron distribution with field aligned electrons traveling both towards and away from Mars. Both electron spike A and B are observed with photoelectrons that are both parallel and anti-parallel to the magnetic field. While electron spikes A and B are observed above 200 km, electron spikes C, D and E are observed below 200 km. At these times pitch angles distributions lack a loss cone since there is a sharp drop in normalized energy flux of electrons from pitch angles of 90°. Such a feature is indicative of the spacecraft being below the mirroring altitude of electrons. That is there is lack of electrons being reflected to form a loss cone before being absorbed by the atmosphere below the spacecraft.

Fig. 3 shows a diverse range of electron pitch angle resolved energy spectra measured during electron spikes B, C, D and E. Note, the spectra have not been corrected for spacecraft potential, which has been derived from SWEA and LPW as between -0.5 V - -3 V for times 06:08:00 UT - 06:13:07 UT and 06:13:29 UT - 06:16:00 UT (Fig. 3(a)-(b) and (e)-(h)) and between -3 V - -4 V for times 06:13:07 UT - 06:13:29 UT (Fig. 3(c)-(d)). It is assumed the distinct peaks in energy flux measured on field-aligned directions both towards and away from Mars during the electron spikes close to photoelectrons energies, 21 eV - 24 eV (solid vertical line) and 27 eV (dashed vertical line), are due to photoelectrons produced by photoionization of carbon dioxide and atomic oxygen [*Frahm et al.*,

©2018 American Geophysical Union. All rights reserved.

Accepted Article

2006]. For electron spikes A, B, C, D and E, 23 SWEA 2s electron energy spectra include coverage of field aligned directions towards and away from Mars. Of these 23 electron energy spectra, 21 were measured with photoelectron peaks in the energy spectra of field aligned electrons traveling towards and away from Mars.

The results described above show magnetic field topology is ambiguous for the cases of dayside electron spikes A to E presented here. Observations support both magnetic field being open where loss cones are observed (electron spikes A and B) and precipitating solar wind/magnetosheath-like electrons are observed (electron spikes B to E) and magnetic field being closed where bi-directional electron pitch angle distributions are observed (electron spike A) and photoelectron peaks observed in both directions along the magnetic field (electron spikes A to E). In order to simplify the discussions that follow we assume electrons spikes A to E occur on closed magnetic fields and that observations of photoelectrons showing closed magnetic field take precedence over conflicting features in support of open magnetic field. The electron energy spectra from Fig. 3(e)-(h) measured during electron spike D and E show, in addition to the peak in photoelectrons, there are peaks in energy flux of more energetic electrons measured around 150 eV and 50 eV respectively. These observations allow for a number of different interpretations. Typically, peaks in electron energy flux at higher energies are indicative of the acceleration of electrons through field aligned potential drop [*Brain et al.*, 2006], which in the case presented here would occur over very brief periods and possibly relate to LPW measurements of strong wave amplitude electric fields on short time scales. The observations alongside photoelectron peaks could indicate the presence of a field aligned potential drop on closed or open magnetic field, where ionospheric electrons traveling away from Mars are reflected by the potential drop to form peaks in photoelectrons traveling towards Mars [*Collinson et al.*, 2015]. Another interpretation is the injection of energetic electrons on closed magnetic fields on the Martian dayside [*Harada et al.*, 2015].

©2018 American Geophysical Union. All rights reserved.

Accepted Article

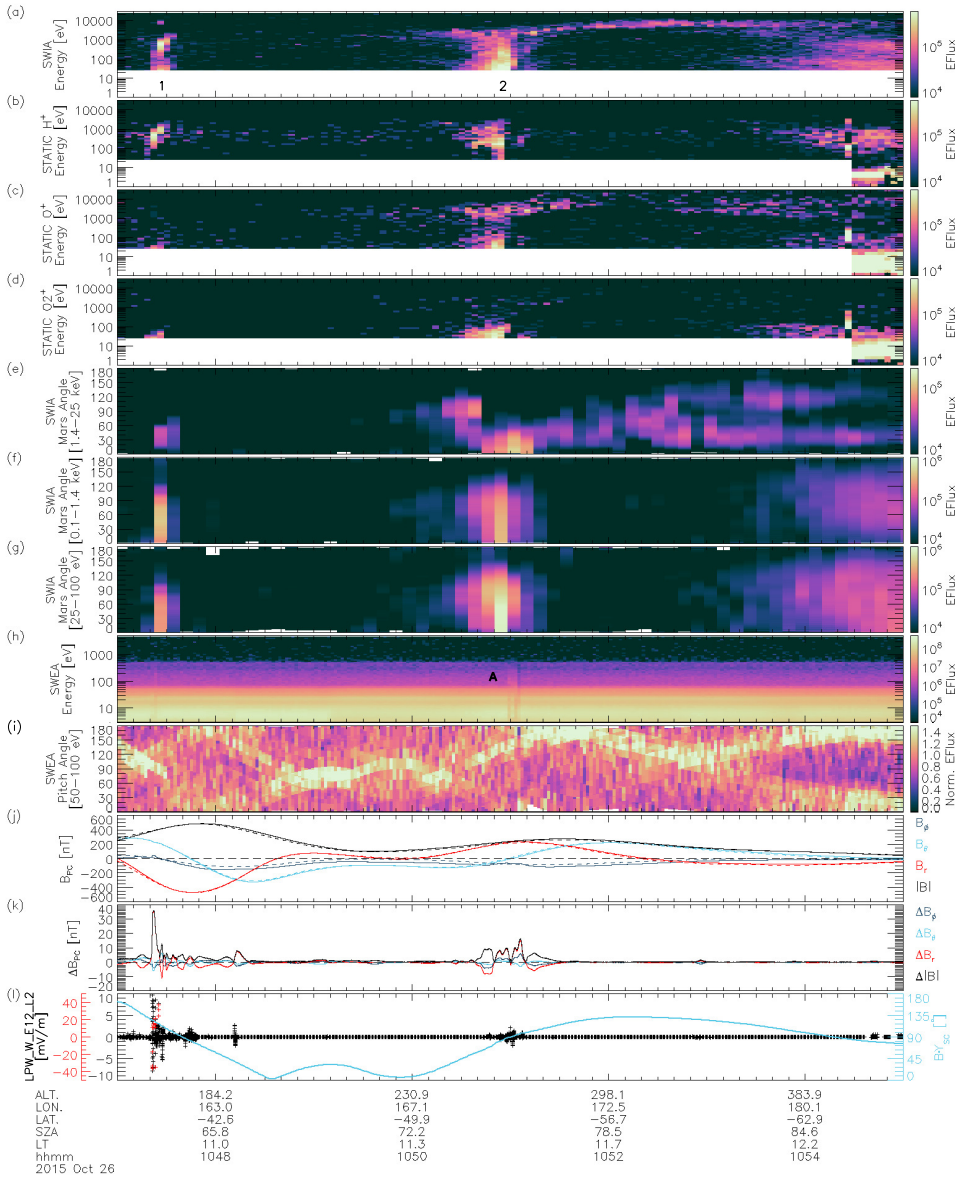

Figure 1. MAVEN observations orbit 2088 on October 26th, 2015, showing broad energy range ion spikes and keV ion bands at altitude <300 km. (a) SWIA omni-directional ion energy flux energy-time spectrogram, (b)-(d) STATIC H^+, O^+ and $O_2{}^+$ omni-directional ion energy flux energy-time spectrogram, (e)-(g) SWIA ion angular distribution functions between 1.4 keV - 25 keV, 0.1 keV - 1.4 keV, and 25 eV - 0.1 keV (0° directed towards Mars), (h) SWEA omni-directional electron energy flux energy-time spectrogram, (i) SWEA electron pitch angle distribution between 50 eV - 100 eV (j) MAG magnetic field vectors in planetocentric co-ordinates, eastward (dark blue), southward (light blue), radial (red) and magnitude (black) compared to the *Morschhauser et al.* [2014] crustal magnetic field model (dotted lines respectively), (k) MAG magnetic field perturbations from background magnetic field in planetocentric co-ordinates and magnitude of perturbation (black), (l) LPW electric field wave amplitude below 10 mV/m (black) and above 10 mV/m (red) and angle between the spacecraft frame Y-axis and the local magnetic field (light blue). Horizontal axis labels show spacecraft altitude, longitude, latitude, solar zenith angle, local time and universal time respectively.

©2018 American Geophysical Union. All rights reserved.

Accepted Article

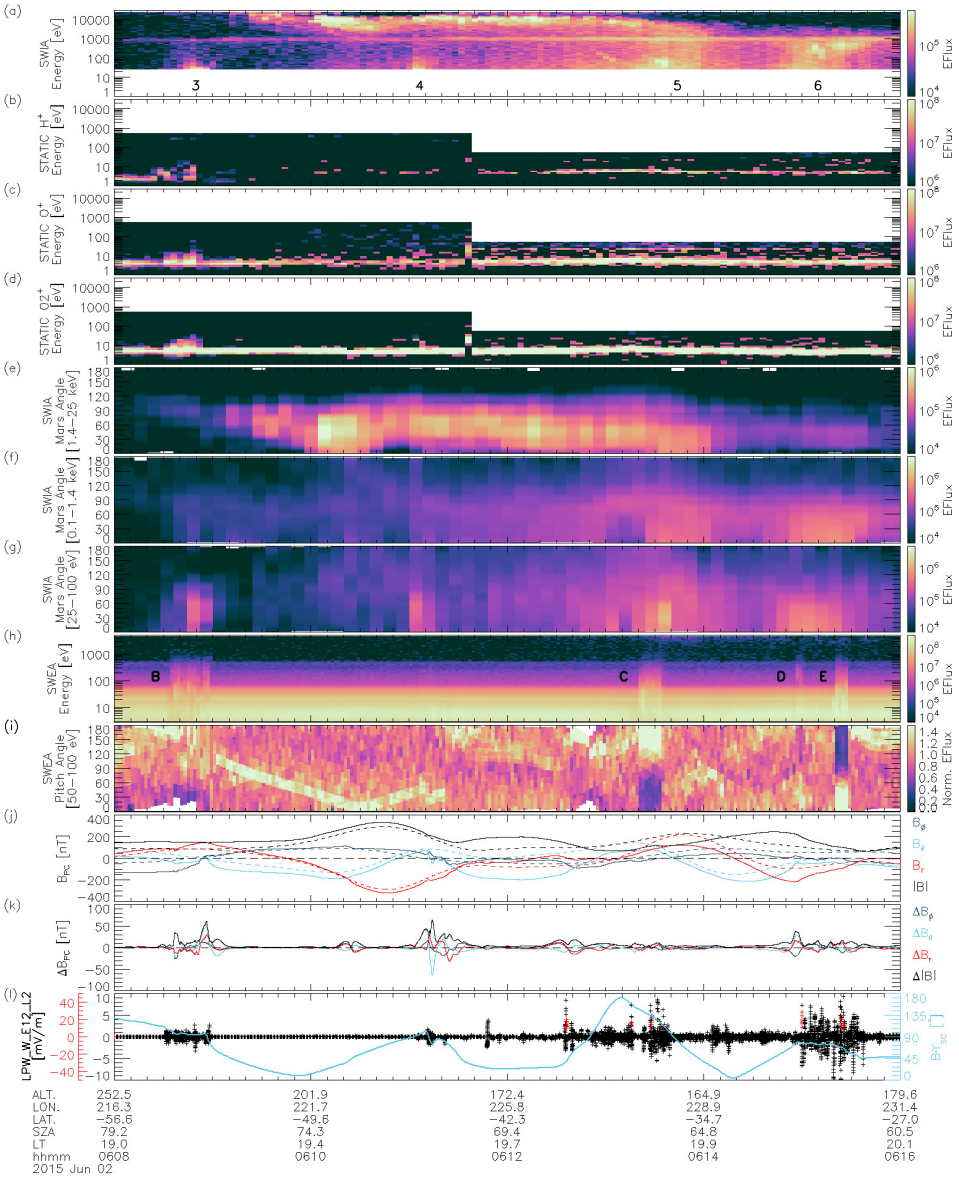

Figure 2. MAVEN observations from orbit 1307 on June 2nd, 2015, showing signatures of broad energy range ion spikes and keV ion bands at altitude <300 km. Figure format identical to Fig. 1.

©2018 American Geophysical Union. All rights reserved.

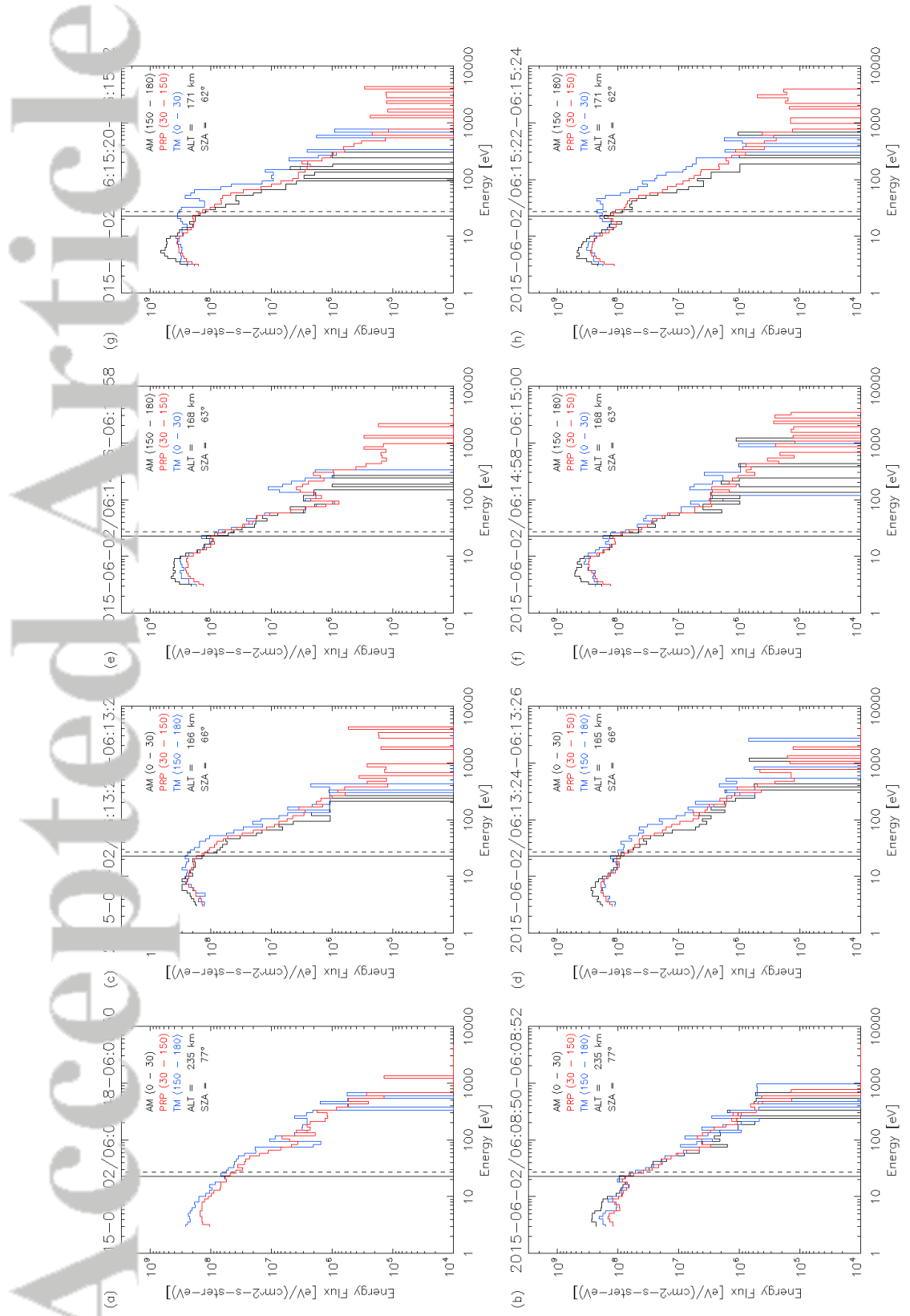

Figure 3. Pairs of consecutive 2s SWEA electron energy spectra showing evidence of closed magnetic field topology and diverse energy spectra during electron spikes B, C, D and E, as well as brief periods of accelerated electrons during electron spikes D and E from orbit 1307 on June 2nd, 2015 (cf. Fig. 2(h)). Electron energy spectra are plotted for field-aligned directions that are most towards Mars in blue (TM), most away from Mars in black (AM) and perpendicular to the magnetic field in red. Vertical lines are also plotted at the CO_2 and O ionization energies around 23 eV and 27 eV (solid and dashed lines respectively) to help identify photoelectron peaks in each spectra. SWEA electron energy spectra have not been corrected for spacecraft potential, which is estimated to be between -0.5 V - -3 V for Fig. 3(a)-(b) and Fig. 3(e)-(h) and between -3 V - -4 V for Fig. 3(c)-(d).

Accepted Article

©2018 American Geophysical Union. All rights reserved.

Accepted Article

5 Characteristics of energetic ions in low altitude closed radial crustal magnetic field on the dayside of Mars

Fig. 4 considers how regions of crustal magnetic field with different magnetic field strengths may cause different energetic ion populations from the induced magnetosphere to precipitate towards Mars. Fig. 4(a) presents a color graph of ion gyroradius as a function of perpendicular energy and magnetic field strength with different color scale axes for H^+, O^+ and $O_2{}^+$ respectively. Highlighted are the perpendicular energies of H^+ (1.2 keV), O^+ (80 eV) and $O_2{}^+$ (40 eV) that results in a gyroradius of 100 km in a 50 nT magnetic field.

In scenario 1 from Fig. 4(b), the gyroradius of ions are sufficiently large compared to the spatial scale of the crustal magnetic fields such that ions are unmagnetized and the magnetic moment of the particle is not conserved as an invariant of motion. Under such conditions, ions that encounter crustal magnetic fields at large pitch angles may penetrate to very low altitudes before being magnetically reflected. Ions that encounter crustal magnetic fields with smaller pitch angles will have less perpendicular energy and be more magnetized and as a result may be deflected into the footpoints of the crustal magnetic field in regions of radial magnetic field. Ions that encounter radial crustal magnetic fields on Marsward / field aligned trajectories will precipitate towards the footpoints. This scenario is analogous to the deflection of solar wind ions by Lunar magnetic anomalies forming regions of enhanced ion density or halos, at the footpoints of the magnetic field [*Kallio et al.*, 2012]. Note, in the case of the Lunar magnetic anomalies, observations show evidence of strong electric fields in regions of remnant magnetic fields [*Saito et al.*, 2012; *Futaana et al.*, 2013], that are also reproduced in models of the solar wind interaction and would contribute to the deflection of ions by the Lorentz force into footpoints of the magnetic field. In this type of interaction, the ion velocity distributions observed above the altitudes where magnetic reflection occurs should be highly asymmetric with respect to the radial direction. That is, beams of ions move towards and beams of reflected ions move away from the magnetic anomalies [*Deca et al.*, 2015].

In scenario 2 and 3 from Fig. 4(c) and (d) respectively, ions precipitating in low altitude regions of the radial crustal magnetic field are shown to have a magnetic connection to higher altitudes on either closed or open magnetic field. Ions at higher altitude with small enough pitch angles will flow along the magnetic field. This can result due to magnetic reconnection as shown in Fig. 4(c) or due to the filling of the loss cone as shown in Fig. 4(d). The latter may occur in the presence of pitch angle scattering effects, which

©2018 American Geophysical Union. All rights reserved.

Accepted Article

could occur when the gyroradius of ions are of similar scale to the crustal magnetic fields or from some wave particle interaction. In both cases shown by Fig. 4(c) and (d), ions that initially have small enough pitch angles may be sufficiently magnetized to conserve the first adiabatic invariant to mirror and reflect at higher altitudes as compared to the unmagnetized ions presented in scenario 2. Particles with this property are adiabatic and as such should satisfy the so-called parameter of adiabaticity being much greater than one [*Grigorenko et al.*, 2009]. The parameter of adiabaticity, κ, was introduced by *Buchner and Zelenyi* [1986] and is defined as the square root of the ratio of the minimum radius of curvature of the magnetic field, R_{cmin}, to the maximum gyroradius of a particle, r_{gmax}, $\kappa=\sqrt{(R_{cmin}/r_{gmax})}$. For $\kappa<1$, particles may adhere to a quasi-adiabatic motion [*Buchner and Zelenyi*, 1989], whereas values of κ approaching unity describe particles that may experience non-adiabatic dynamics that are subject to chaotic motion and particle scattering. Note, in the example of Fig. 1(j), there is 12° of latitude that separates the maximum radial magnetic field measured at 10:47:45 UT and 10:51:06 respectively, which is equivalent to a radius of curvature of around 370 km at an altitude of 180 km and a κ of around 2 for r_{gmax} = 100 km. Therefore, the adiabatic behavior of energetic ions is not to be expected for regions of crustal magnetic fields observed here. Rather, pitch angle scattering effects may be expected.

Note, the possibility for adiabatic behavior in low altitude crustal magnetic field regions will be counteracted as ion-neutral collisional frequency increases as altitude or solar zenith angle decreases. That is, when the ion gyrofrequency to ion-neutral collisional frequency is equal to or less than unity ions are considered unmagnetized. Unfortunately, neutral density measurements from the MAVEN Neutral Gas and Ion Mass Spectrometer (NGIMS) [*Mahaffy et al.*, 2015a] were not available for time periods considered here. However, in sections 5.1 and 5.2 we estimate the ratio of ion gyrofrequency to ion-neutral collisional frequency using an updated version of Figure. 4 from *Mahaffy et al.* [2015b] of the distribution of the average CO_2 neutral density measured by NGIMS as a function of solar zenith angle and altitude using 13 months of data November, 2015 to end of December, 2016.

The following discussion investigates the 3D field of view (FOV) ion distributions and 2D ion velocity distributions during ion spike 2 and 5 and ion spike 1 and 6 respectively. The 3D FOV ion distributions have been centered on Mars and the 2D ion velocity distributions have been organized with respect to the magnetic field direction such that

©2018 American Geophysical Union. All rights reserved.

Accepted Article

parallel velocities are plotted along the horizontal axis. The 2D ion velocity distribution interpolates and smooths over data points gathered in a ±20° polar angular range about the magnetic field direction. The plane of the 2D ion velocity used is that which best resolves the parallel ion beam and is not oriented with respect to the direction of the local convective electric field. Both 3D FOV and 2D ion velocity distributions have been corrected for spacecraft velocity. The 3D FOV and 2D ion velocity distributions are not corrected for spacecraft potential or bulk velocity. We do not expect the inclusion of a spacecraft potential of a few volts and a bulk velocity dominated by the cold ion population below 10 eV (not measured by STATIC) to produce any significant difference for velocity distributions of ions measured above 25 eV.

5.1 Precipitating 25 eV -1.4 keV flowing-ion and keV ion-beam distributions

Fig. 5 compares SWIA 3D FOV ion distributions and SWIA 2D ion velocity distributions between 10:50:52 UT - 10:50:56 UT, October 26th, 2015 and during ion spike 2. Fig. 6 compares SWIA 3D FOV ion distributions and SWIA 2D ion velocity distributions during ion spike 5 and between 06:13:42 UT - 06:13:46 UT, June 2nd, 2015. The figures show ion distributions from three energy ranges 1.4 keV - 25 keV, 0.1 keV - 1.4 keV and 25 eV - 0.1 keV. The different energy ranges have been chosen to reflect the different ion populations identified by STATIC during ion spike 1 and 2 (cf. Fig. 1(b)-(d)).

Fig. 5(a)-(b) shows that during ion spike 2, ions E>1.4 keV associated with O^+ ions, are characterized by a clear narrow anti-parallel beam of ions directed towards Mars. This is indicative of ions accelerated externally that have been injected into the local region. Whereas during ion spike 5, Fig. 6(a)-(b) shows ions E>1.4 keV are characterized by a distribution of field aligned ions directed towards Mars, that extends between velocities corresponding to energies of 0.3 keV - 4.5 keV. This is indicative of a local heating process, but it is unknown if this is a result of a local energization or deceleration process. Examples of the latter are observed in cases of deceleration of solar wind ions at the Lunar magnetic anomalies [*Saito et al.*, 2012].

In terms of ions E>1.4 keV associated with O^+ ions, the distinct beams of accelerated and heated ions precipitating towards Mars are indicative of the type of interaction presented by Fig. 4(b), where the ion gyro-forces are less important. Further aspects of this precipitation is discussed in sections 6 and 7.

©2018 American Geophysical Union. All rights reserved.

Accepted Article

Fig. 5(c)-(f) shows ions associated with H^+ ions between 0.1 keV - 1.4 keV and ions associated with O^+ and $O_2{}^+$ between 25 eV - 0.1 keV are characterized by an asymmetrical distribution where larger phase space densities are observed alongside a broad velocity distribution in the anti-parallel hemisphere directed towards Mars. This feature is also reproduced during ion spike 5 as shown in Fig. 6(c)-(f). Fig. 5(d) shows ions associated with H^+ ions between 0.1 keV - 1.4 keV occur with distinctly different distributions above and below a velocity of 250 km/s (320 eV). Below 250 km/s the ion velocity distribution shows higher phase space density and is more isotropic in the anti-parallel direction, whereas above 250 km/s the distribution is more structured and fragmented. Fig. 5(f) shows ions between 25 eV - 0.1 keV as associated with O^+ and $O_2{}^+$ ions, display a similar fragmented structure to the distribution above 250 km/s from Fig. 5(d). A fragmented structure observed in ion velocity distributions is indicative of non-adiabatic effects and have been modeled by *Martin et al.* [2000] as well as observed by *Vaisberg et al.* [2015] in regions of the Earth magnetosphere where non-adiabatic effects are important.

In comparison, Fig. 6(d) and (f) shows that during ion spike 5, the anti-parallel distribution of ions precipitating towards Mars is generally less structured. However, there is a more appreciable component of ions directed away from Mars. This includes narrow components of enhanced phase space density aligned along the Sunward direction over a wide range of velocity and beams of ions at lower velocity that are oblique to the magnetic field direction and directed away from Mars (cf. Fig. 6(d) and (f)). Note, Fig. 6(e) shows a distinct beam of ions in the anti-Sunward direction that most likely correspond to penetrating solar wind protons.

In terms of ions E<1.4 keV, the similar broad ion velocity distribution for ions between 0.1 keV - 1.4 keV and 25 eV - 0.1 keV, would suggest the ion populations between these energy ranges have been transported from similar regions at higher altitudes with some magnetic connection between regions of crustal magnetic field at higher altitudes and radial magnetic field footpoints at lower altitude. This would indicate the type of interaction presented by Fig. 4(c) and (d), where the ion gyro-forces are of greater importance. This is supported by the observations of a reflected component of ions directed away from Mars (cf. Fig. 5(c)-(f) and Fig. 6(c)-(f)). Indeed, Fig. 5(c)-(f) shows in the case of ion spike 2, in the parallel hemisphere directed away from Mars, is a sharp drop in phase space density for an approximately constant angle about the parallel axis over both, 25 eV - 0.1 keV and 0.1 keV - 1.4 keV, energy ranges. Such a feature is indicative

©2018 American Geophysical Union. All rights reserved.

Accepted Article

of an ion loss cone and supports a conservation of the first adiabatic invariant and also raises the prospects of ions being absorbed by the Martian atmosphere. That is losing energy through collisions, contributing to the sputtering process and also possibly resulting in auroral emissions. However, the parameter of adiabaticity does not support adiabatic effects during the time of Fig. 5(a)-(b). If assuming a magnetic field radius of curvature of 370 km and considering magnetically reflected H^+ ions between, 0.1 keV - 1.4 keV and O^+ and $O_2{}^+$ ions between, 25 eV - 0.1 keV, results in values of κ ranging from 3 to 8.

In the case of Fig. 5(d) and (f), evidence of magnetic mirroring is observed around 260 km at a time STATIC data is available to identify different ion species. Using NIGMS 2015 average data, the ratio of ion gyrofrequency to ion-neutral collision frequency is much greater than unity at this altitude and SZA and remains greater than unity down to altitudes of 147.5 km or lower for H^+, 152.5 km for O^+ and 162.5 km for O_2^+. However, a loss cone of 45° at a measured magnetic field strength of around 220 nT gives a mirroring field strength of around 450 nT, which corresponds to an altitude of around 150 km if using the *Morschhauser et al.* [2014] model. Therefore, it seems plausible as long as the parameter of adiabaticity is sufficiently large, the observed populations of O^+ with E>25 eV and H^+ with E>0.1 keV will remain magnetized down to the mirror altitude.

In the case of Fig. 6(d) and (f), Fig. 6(d) does not show any obvious loss cone, although there is an appreciable reflected component that is asymmetrical about the parallel axis. Fig. 6(f) shows a more defined loss cone that is symmetrical about the parallel axis at around 57° pitch angle. At lower pitch angles and within the loss cone, there are ions moving away from Mars in a conic-like distribution that is symmetrical about the parallel axis and is suggestive of ions being mirrored up the field line. Using NIGMS 2015 average data, the ratio of ion gyrofrequency to ion-neutral collision frequency is greater than unity at this altitude and SZA and remains greater than unity down to altitudes of 147.5 km or lower for H^+, whereas the ratio is less than unity for O^+ and O_2^+ at the altitude at observation. Therefore, O^+ and O_2^+ are expected to be unmagnetized at this time and would not be expected to result in the evidence of magnetic mirroring in Fig. 6(f). Instead, such features may result from the presence of H^+ ions between 25 eV - 0.1 keV, but are not possible to identify due to the lack of STATIC measurements at this time. Also, as the observed magnetic field (|B|~130 nT) is much perturbed compared to the *Morschhauser et al.* [2014] model (|B|~230 nT) it is not possible to determine if a population H^+ ions are magnetized down to the mirroring altitude at this time.

©2018 American Geophysical Union. All rights reserved.

Accepted Article

The precipitation of ions and electrons in regions of radial magnetic field where ions show signs of conserving the first adiabatic invariant lends itself to the comparison of similar features observed in the dayside cusp region at the Earth, where open reconnected magnetic field leads to the precipitation of electrons and ions and the mirroring of ions [*Onsager et al.*, 1993; *Bouhram et al.*, 2002]. Similar ion velocity distributions are also observed at Mercury showing flowing ion distributions of magnetosheath plasma precipitating in the cusp regions [*Raines et al.*, 2014]. Moreover, models of the solar wind interaction with Mars have also shown how magnetosheath plasma may flow along open field lines to become focused in cusps of the Martian crustal magnetic fields [*Brecht and Ledvina*, 2012].

However, given the interpretation of SWEA electron measurements showing closed magnetic field during the ion spikes reported here, the ion velocity distributions presented here are interpreted as ions flowing along closed magnetic field lines from higher altitude crustal magnetic field. This is supported by the energy-mass composition of ions associated with ion spikes 1 and 2 also being observed above ~390 km during the same periapsis pass and in a region of more horizontal crustal magnetic field (after 10:54:00 UT in Fig. 1(a)-(d)). Fig. 4(c) presents one possible explanation involving the reconnection of once open crustal magnetic fields forming closed magnetic field and Marsward flows of ions [*Harada et al.*, 2015].

Fig. 4(d) presents another possible explanation involving the filling in of the ion loss cone. The later may occur from the pitch angle scattering and isotropization of flows of ions from the induced magnetosphere that have drifted on to crustal magnetic fields. A similar case has been successfully modeled to explain ion precipitation on closed magnetic field of the dayside polar region of the Earth magnetosphere [*Alem et al.*, 1995]. Unfortunately, without further observations or simulations, it is difficult to differentiate between ions that are precipitating as a result of magnetic reconnection or ions precipitating as a result of the filling of the loss cone. In any case, further study of ion spikes in regions of radial crustal magnetic field could prove an important tool for the remote sensing of processes related to magnetic reconnection or non-adiabatic effects of crustal magnetic fields.

Depending on the energy of the ions the interaction with the Martian crustal magnetic fields has properties in common with Lunar type interaction presented in Fig. 4(b) and scenario 1, where precipitating ions above 1.4 keV are beam like. However, below 1.4

©2018 American Geophysical Union. All rights reserved.

keV the ion interaction seems quite unlike the Lunar example and instead points to greater magnetization above the mirroring altitude and reflects the type of interaction presented in Fig. 4(c) and (d) and scenario 2 and 3.

Accepted Article

©2018 American Geophysical Union. All rights reserved.

Accepted Article

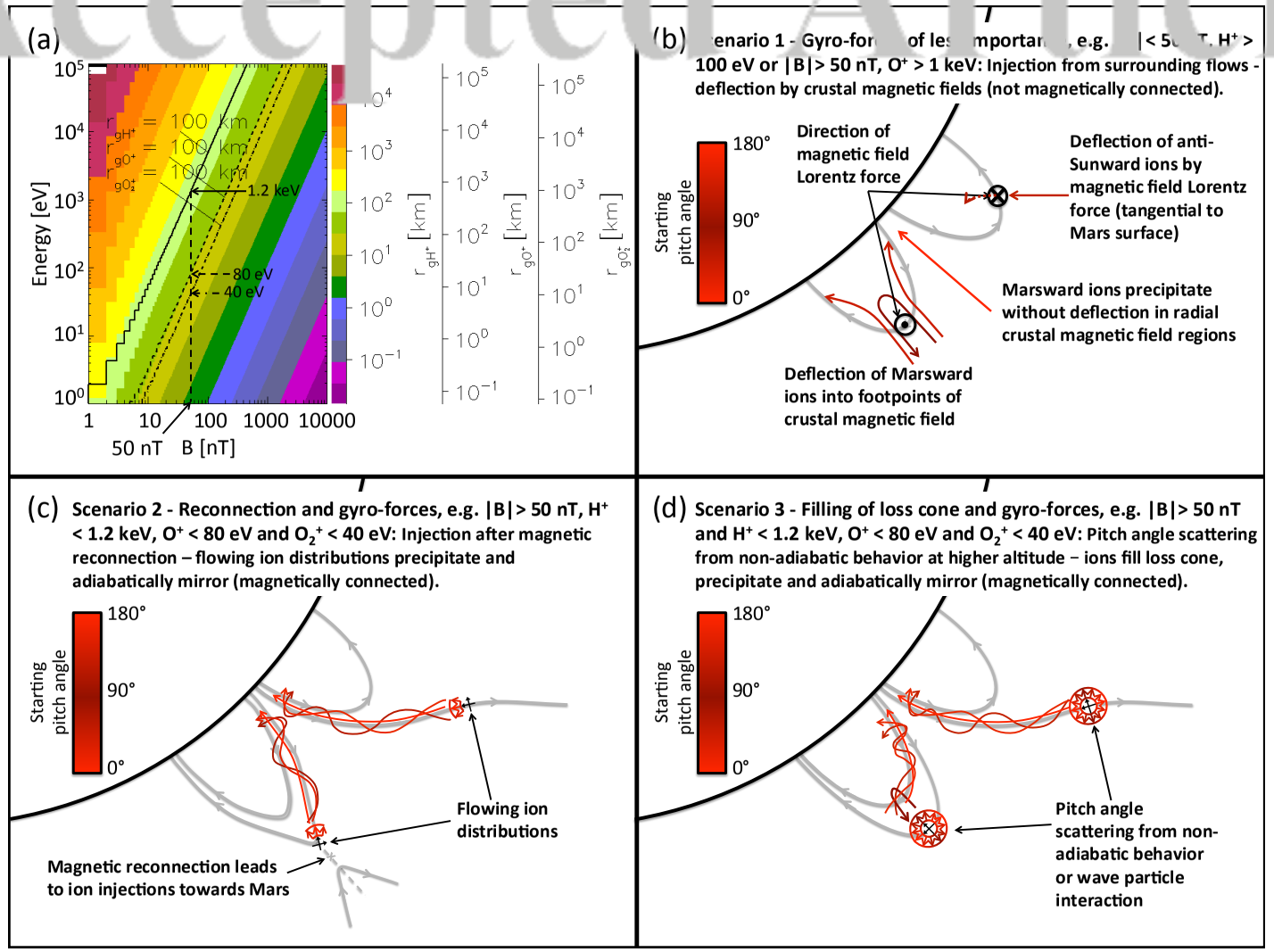

Figure 4. Effects of ion gyroradius on the interaction of ions moving towards the Martian crustal magnetic fields. (a) Color graph of ion gyroradius as function of perpendicular energy and magnetic field strength with different color scale axes for H^+, O^+ and O_2^+ respectively. (b) Scenario 1 - finite gyroradius effects of H^+ ions E>100 eV moving towards regions of weak crustal magnetic fields or O^+ ions E>1 keV moving towards both weak or strong crustal magnetic fields. (c) Scenario 2 - precipitation of field aligned flows of different ion populations due to magnetic reconnection. (d) Scenario 3 - precipitation of field aligned flows of different ion populations due to filling of the ion loss cone.

©2018 American Geophysical Union. All rights reserved.

Confidential manuscript submitted to *JGR-Space Physics*

Accepted Article

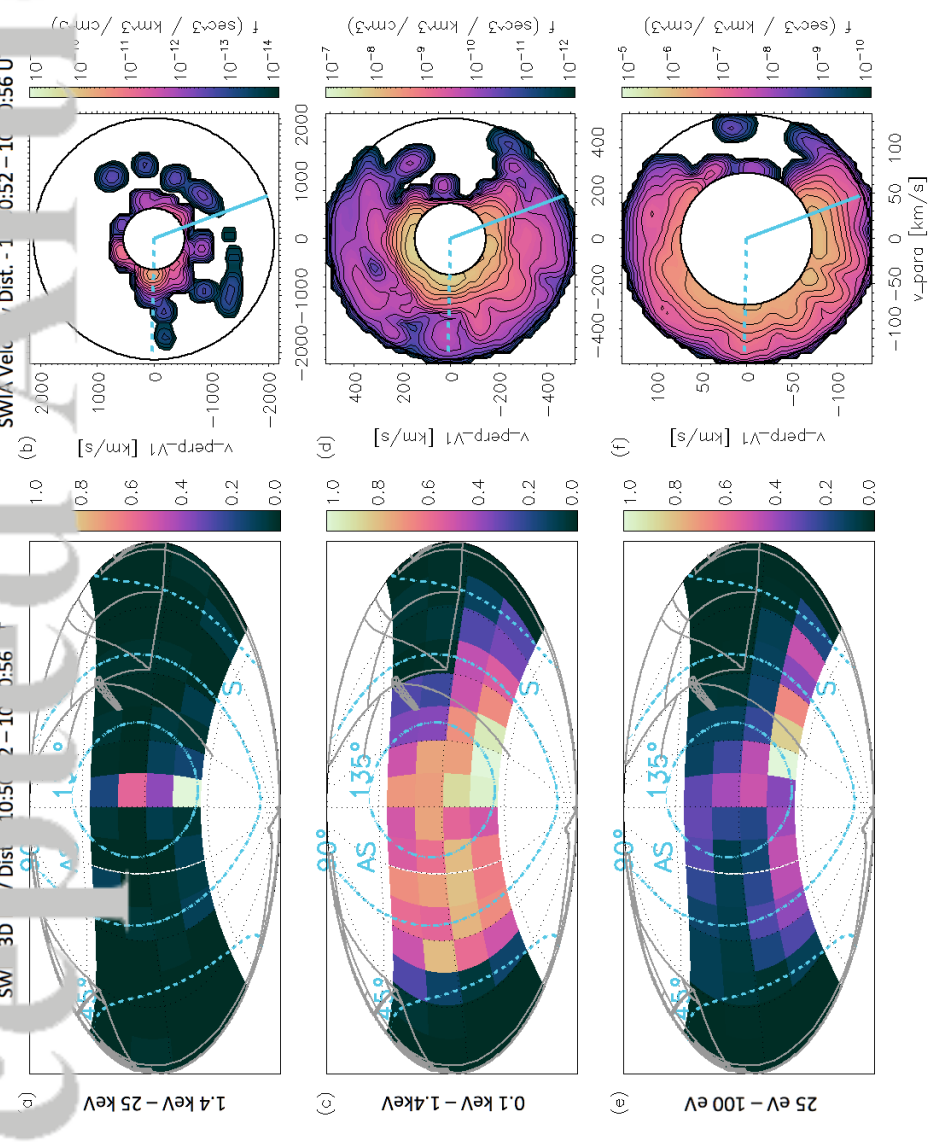

Figure 5. Comparison of SWIA 3D field of view (FOV) ion distributions (left-hand column of panels) and SWIA 2D ion velocity distributions (right-hand columns of panels) over three energy ranges 1.4 keV - 25 keV (top row), 0.1 keV - 1.4 keV (middle row) and 25 eV - 0.1 keV (bottom row) between 10:50:52 UT - 10:50:56 UT, October 26th, 2015 and during ion spike 2. Note, during this period the magnetic field is mostly radial with elevation angles of 68° - 72°. SWIA 3D FOV ion distributions are centered on Mars and include labels for Sunward (S) and anti-Sunward (AS) directions, as well as light blue contours to show angles of 45°, 90° and 135° from the magnetic field direction. A grey outline is used to illustrate the MAVEN spacecraft in the instrument FOV. Right-hand column of panels show the SWIA 2D ion velocity distributions in a plane consisting of velocity parallel to the magnetic field along the horizontal axis and velocity perpendicular to the magnetic field along the vertical axis. Solid and dashed light blue lines show directions towards the Sun and Mars respectively. SWIA 2D ion velocity distributions axes show velocities for H^+ ions (the velocity of O^+ and O_2^+ ions may be obtained by dividing values on axes by 4 and 5.65 respectively).

©2018 American Geophysical Union. All rights reserved.

Accepted Article

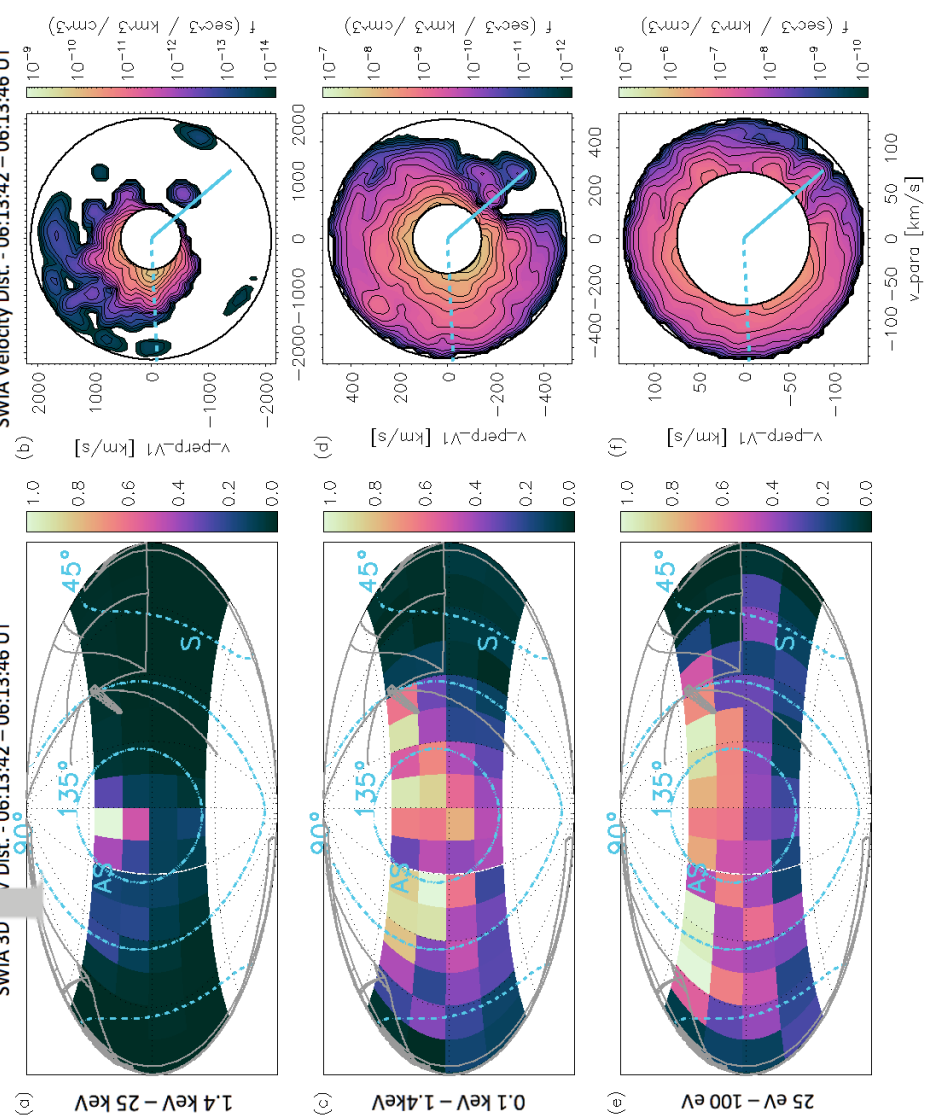

Figure 6. Comparison of SWIA 3D FOV ion distributions (left-hand column of panels) and SWIA 2D ion velocity distributions (right-hand columns of panels) over three energy ranges 1.4 keV - 25 keV (top row), 0.1 keV - 1.4 keV (middle row) and 25 eV - 0.1 keV (bottom row) between 06:13:42 UT - 06:13:46 UT, June 2nd, 2015 and during ion spike 5. During this time MAVEN is situated in a region of radial crustal magnetic field with local elevation angle of 74° - 85°. Format of 3D FOV ion distributions and 2D ion velocity distributions follows that from Fig. 5.

©2018 American Geophysical Union. All rights reserved.

Accepted Article

5.2 Downward mirroring ions and upward ion conics

Fig. 7 shows SWIA 3D FOV and 2D ion velocity distributions associated with H^+ ions between 0.1 keV - 1.4 keV during ion spike 1 and 6. Both ion spikes 1 and 6 show field aligned distributions of ions with a high phase space density spread over a wide range of parallel velocity precipitating towards Mars (cf. Fig. 7(b) and (d)). The SWEA 3D FOV and 2D electron velocity distributions during electron spike E is also shown to highlight the remarkable similarity in the 3D FOV of SWIA and SWEA during ion spike 6 showing the simultaneous field aligned precipitation of ions and electrons towards Mars (cf. Fig. 7(e)-(f)).

During ion spike 1 and 6, but most pronounced during ion spike 1 (cf. Fig. 7(b)), the ion velocity distributions show departure from field aligned angles for increasing parallel velocity leading to a broad distribution that is asymmetrical about the parallel direction. The distribution of larger ion phase space density extends out to larger pitch angles along the negative perpendicular axis for increasing parallel velocity. Also in both cases of ion spike 1 and 6, the observed characteristics described in the parallel hemisphere are reproduced for ion velocity distributions over nearly 90° polar angle revolution around the parallel direction (not shown). Combined with an asymmetry in the perpendicular direction, the velocity distribution of the precipitating ions of Fig. 7(b)) and (d) represents a non-gyrotropic partial ion ring distribution about the magnetic field. Ion ring velocity distributions observed for downflowing ions in the magnetic field cusp region of the Earth are considered to demonstrate the conservation of the first adiabatic invariant in a converging mirror field [*Gorney*, 1983]. Therefore, the above observation of a partial ion ring distribution would be the first evidence of a similar process in the crustal magnetic fields of Mars.

The observation of ion mirroring for the energy range associated with H^+ ions in regions of the radial crustal magnetic field of Mars is an important part of understanding the dynamics of the Martian radial crustal magnetic field / cusps. First, it illustrates further how energetic ions (H^+ ions) are at least partially magnetized in regions of crustal magnetic field despite the parameter of adiabaticity not supporting adiabatic effects during these time periods. For example, assuming a 370 km magnetic field radius of curvature and H^+ ions observed as mirroring mostly below 830 eV, κ is around 6 during the time of Fig. 7(a)-(b) and is around 3 during the time of Fig. 7(c)-(d). The adiabatic behavior

©2018 American Geophysical Union. All rights reserved.

Accepted Article

observed in the ion velocity distributions presented here and in section 5.1 is contrary to the expected lack of adiabatic behavior from the radius of curvature of the crustal magnetic field currently being considered. This would suggest different ions populations are injected onto crustal magnetic fields with mostly field aligned distributions and have low enough perpendicular velocity to ensure some adiabatic behavior. Alternatively, the radius of curvature of the crustal magnetic field that has been considered could be significantly underestimated at a few hundred kilometers.

Second, the observation of electrons and different ion species mirroring at different altitudes in the crustal magnetic field cusps raises the prospect of a charge separation dynamo and associated parallel electric fields forming in these regions. However, in the regions of radial crustal magnetic field and periods of ion spikes presented here, LPW's single axis measurements did not provide coverage along the magnetic field and measured large electric field wave amplitudes at perpendicular to oblique angles to the magnetic field. Ion spike 1 and 6 for which mirroring ions are observed, occur at 175 km and 173 km respectively. This compares to electron spike B observed with a loss cone and above 200 km and electron spike C, D and E observed without a strong mirroring of electrons or a loss cone at 164 km, 169 km and 173 km respectively. Fig. 8(a) summarizes such observations and shows how the difference in altitudes where energetic electrons (blue arrows, negative symbols and energy distributions) and H^+ ions (red arrows, positive symbols and energy distributions) in regions of radial crustal magnetic field may lead to some amount of charge separation, allowing a charge separation dynamo and associated parallel electric fields to form (represented by black arrow and $E_{\parallel}$). Such a process would also support the presence of large wave amplitude electric fields as measured by LPW and also field aligned currents as related to the large magnetic field perturbations measured by MAG.

Third, the non-gyrotropic partial ion ring distributions observed as part of the mirroring H^+ ion velocity distributions could be unstable to plasma wave instabilities resulting in the energization of ions in analogy to similar velocity distributions observed in the dayside cusp region at Earth [*Cattell and Hudson*, 1982; *Roth and Hudson*, 1985; *Hudson and Roth*, 1986]. Indeed, the ion velocity distribution presented from ion spike 6 shows the simultaneous observation of downflowing ions and upflowing ions, which occur at quite conical pitch angles about the magnetic field and indicate a transverse ion energiza-

©2018 American Geophysical Union. All rights reserved.

Accepted Article

tion and ion outflow process similar to that observed for the Earth cusp (*Øieroset et al.* [1999] and references therein).

Fourth, while the observations of precipitating heavy ions may result in atmospheric escape from energy deposition and sputtering, mirroring H^+ ions in low altitude radial crustal magnetic field may also aid atmospheric escape from Mars through the charge exchange process. As shown in Fig. 8(a) a mirroring H^+ ion may charge exchange with the background neutral atmosphere forming an energetic neutral hydrogen atom that is able to escape from Mars. This would be analogous to similar processes thought to occur at Earth [*Roelof*, 1997]. This could also explain MEX observations showing an enhancement of hydrogen ENA flux in the presence of crustal magnetic fields on the dayside of Mars [*Wang et al.*, 2014]. The formation of an hydrogen ENA in the above process would potentially lead to the escape of this hydrogen from Mars. Therefore, ignoring the effects of sputtering caused by the precipitating H^+ ions, which is marginal compared to that caused by the precipitation heavier ions such as the planetary O^+ ions, the escaping ENA formed by the charge exchange process on the precipitating H^+ ions could represent an additional escape of planetary hydrogen from Mars if the original source of the precipitating H^+ ions is from the hot ion corona of Mars instead of the solar wind.

This study also presents the first such measurements at Mars by MAVEN's LPW, of large fluctuating large electric field wave amplitudes in regions of radial crustal magnetic field and during observations of ion spikes. Although LPW lacks coverage in the direction aligned with the magnetic fields during these periods, the fluctuations of electric fields perpendicular to the magnetic field could also involve oppositely directed electric fields that are adjacent to each other as related to possible small scale double layer structures and associated parallel electric fields [*Block*, 1988]. Unfortunately, as LPW is unable to determine the vector direction of the DC electric field and therefore also an accurate baseline electric field, it is not possible to determine where changes in the sign of the electric field wave amplitude corresponds to changes in the electric field direction.

However, there is some correspondence between increasing electric field wave amplitudes in regions of the crustal magnetic field cusps and the angle of LPW measurements deviating slightly from angles perpendicular to the magnetic field. This might serve as some indication for the strong parallel components in the electric field wave amplitude not covered by LPW in regions of the crustal magnetic field cusps. The presence of small

©2018 American Geophysical Union. All rights reserved.

Accepted Article

scale fluctuations in the parallel electric field is supported by the brief observations during electron spikes D and E of additional energetic peaks in electron energy flux (cf. Fig 3 (e)-(h)). Due to the small gyroscales of electrons the small scale variations in the field aligned electric field potential may act as a DC accelerating field of electrons over small scales. However, such small scale electric fields will be in competition with plasma drifts that move electrons in and out of the small scale potential structures. This may explain why electron energy spectra are measured with a mixture of peaks of accelerated electrons in addition to unaccelerated but heated electron spectra.

Also, the periods of increased electric field wave amplitude fluctuations during ion spike 1 and 6 coincide with ion velocity distributions showing the possible conservation of the first adiabatic invariant by H^+ ions in a magnetic field mirror field. Perpendicular electric fields may produce perpendicular energization of ions through transverse wave heating [*André and Yau*, 1997], acceleration of non-adiabatic ions [*Cole*, 1976] or a combination of both [*Lindstedt et al.*, 2010]. This may relate to characteristics of Fig. 7(b) and (d) showing parallel ions directed towards Mars extending asymmetrically to larger pitch angles for increasing parallel velocity and ions traveling at away from Mars at conical pitch angles [*André and Yau*, 1997; *Øieroset et al.*, 1999].

©2018 American Geophysical Union. All rights reserved.

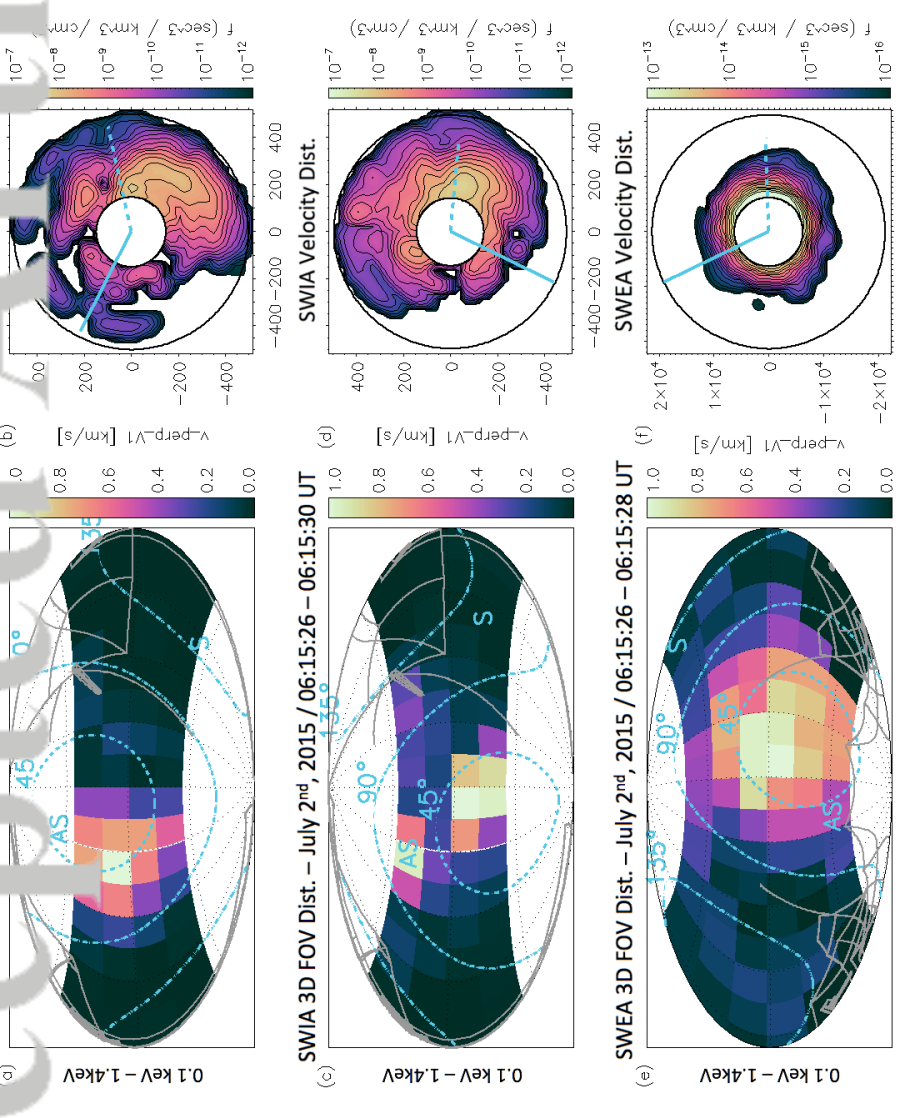

Figure 7. SWIA and SWEA 3D FOV ion and electron distributions (left-hand column of panels) and 2D ion and electron velocity distributions (right-hand columns of panels) between the energy range 0.1 keV - 1.4 keV showing the conservation of the first adiabatic invariant by ions in a magnetic field mirror field. (a)-(b) SWIA ion distributions obtained during ion spike 1 and between 10:47:24 UT - 10:47:28 UT on October 26th, 2015. During this time the magnetic field elevation angle varies between -63° - -55°. (c)-(d) SWIA ion distributions obtained during ion spike 6 and between 06:15:26 UT - 06:15:30 UT, June 2nd, 2015. During this time the magnetic field elevation angle varies between -58° - -40°. (e)-(f) SWEA electron distributions during electron spike E and between 06:15:26 UT - 06:15:28 UT. During this time the magnetic field elevation angle varies between -58° - -48°. Format of 3D FOV ion and electron distributions and 2D ion and electron velocity distributions follow that from Fig. 5.

©2018 American Geophysical Union. All rights reserved.

Accepted Article

Accepted Article

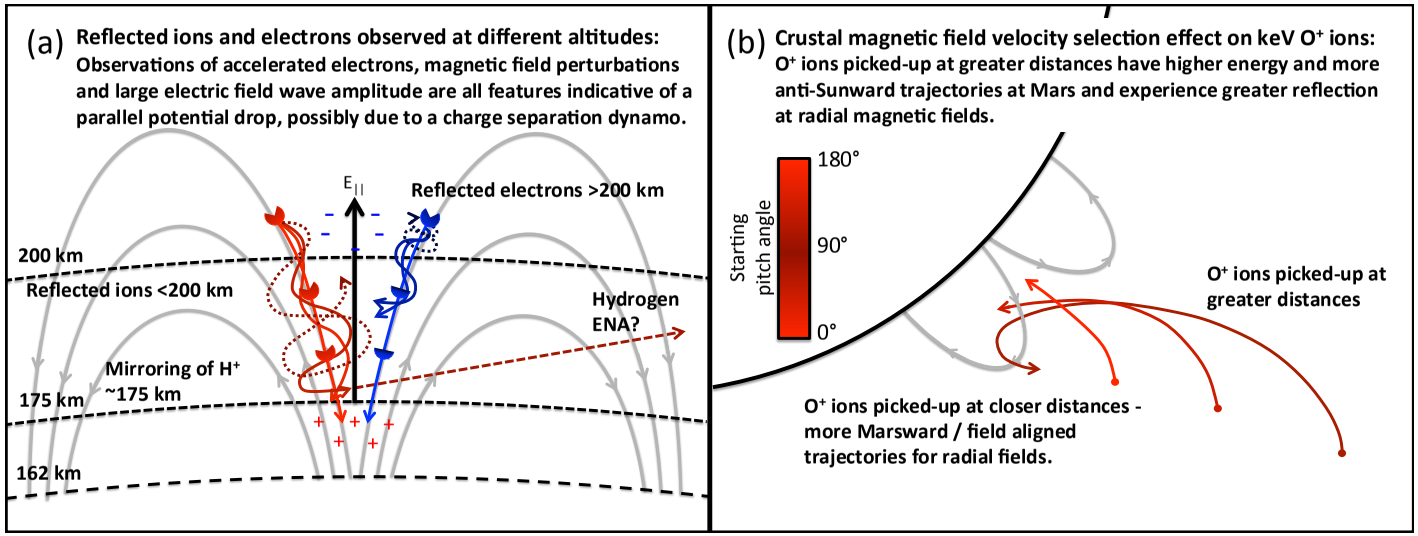

Figure 8. Schematics summarizing (a) how the different altitudes where reflected electrons and ions occur may lead to formation of a charge separation dynamo and parallel electric field potential drop as well as the production of ENA hydrogen from the mirroring of H^+ ions (b) velocity selection effect of keV O^+ ions in regions of low altitude radial crustal magnetic field. Note, particle trajectories with darker shades represent particles that have a larger pitch angle when initially interacting with the Martian crustal magnetic fields.

©2018 American Geophysical Union. All rights reserved.

Confidential manuscript submitted to *JGR-Space Physics*

Accepted Article

6 Spatial ion energy dispersions of keV ions

Fig. 9 shows energy-time spectrograms using a linear energy scale shown on the left-hand axis to highlight the appearance of energy dispersed structures from keV ions observed between the appearance of ion spike 2 and 5 and respective keV ion bands observed close to each ion spike. This is compared to the altitude of MAVEN as shown by the dashed line and right-hand axis. The ion energy dispersions show hallmarks of a presence of electric fields. First is the linear dependence of ion energy (E/q) with time and altitude and second the tone of the energy dispersion is arranged with the spacecraft motion with respect to Mars. Such features have been reported in cases of energy dispersed structures showing the extraction of ions from the Martian magnetosphere by large electric fields [*Dubinin et al.*, 2006a]. However, the energy dispersed structures reported here are for ions precipitating towards Mars and would therefore be related to the deceleration of ions rather than the acceleration of ions described by *Dubinin et al.* [2006a]. The form of the energy dispersed ions reported here at energies >1.4 keV also follow features of modeled solar wind proton energy spectrum showing the deceleration by large electric fields of solar wind protons directed towards magnetic anomalies on the Lunar surface [*Giacalone and Hood*, 2015; *Poppe et al.*, 2016].

In the case of energy dispersion of ions E>1.4 keV on October 26th, 2015, there is a change in 4.75 keV ion energy over 62 km in altitude and approximately 372 km along the MAVEN flight path (93 s at 4 km/s). This would relate to electric fields as large as ~80 mV/m in the radial extent and ~10 mV/m along the orbit path of MAVEN. In the case of energy dispersion of ions E>1.4 keV on June 2nd, 2015, there is a change in 9 keV ion energy over 3.2 km in altitude and approximately 240 km along the MAVEN flight path (60 s at 4 km/s). This would relate to electric fields as large as ~3 V/m in the radial extent and ~40 mV/m along the orbit path of MAVEN. It does not seem conceivable electric fields this large can be present over the scale size of the observed ion energy dispersions without the occurrence of other noticeable effects. For example, the bulk acceleration of the local thermal ion population away from Mars or an equivalent acceleration of electrons towards Mars might be expected but are not observed.

Instead, the energy dispersed structures presented here for ions E>1.4 keV could be interpreted as the velocity selection effect illustrated in Fig. 8(b), due to a combination of the orientation of the magnetic field and trajectories of pick-up ions with different en-

©2018 American Geophysical Union. All rights reserved.

Accepted Article

ergies. In this interpretation O^+ pick-up ions that have spent more time being accelerated in the pick-up process have higher energy and are on more anti-Sunward trajectories and will experience magnetic reflection when encountering regions of stronger radial crustal magnetic field. This could then account for the cut-off in time of higher energy ions (e.g. E>4 keV) in the keV ion-band feature. Whereas O^+ pick-up ions that have spent less time being accelerated have lower energy and are on trajectories that are more directed towards Mars. These ions will be preferentially selected in radial crustal magnetic field regions due to their field aligned pitch angles resulting a beam of keV ions precipitating towards Mars. The tone of energy dispersion could relate to the direction of MAVEN with respect to Mars and altitude since energetic anti-Sunward ions will experience greater magnetic reflection from the increased crustal magnetic field strengths at lower altitudes.

©2018 American Geophysical Union. All rights reserved.

Accepted Article

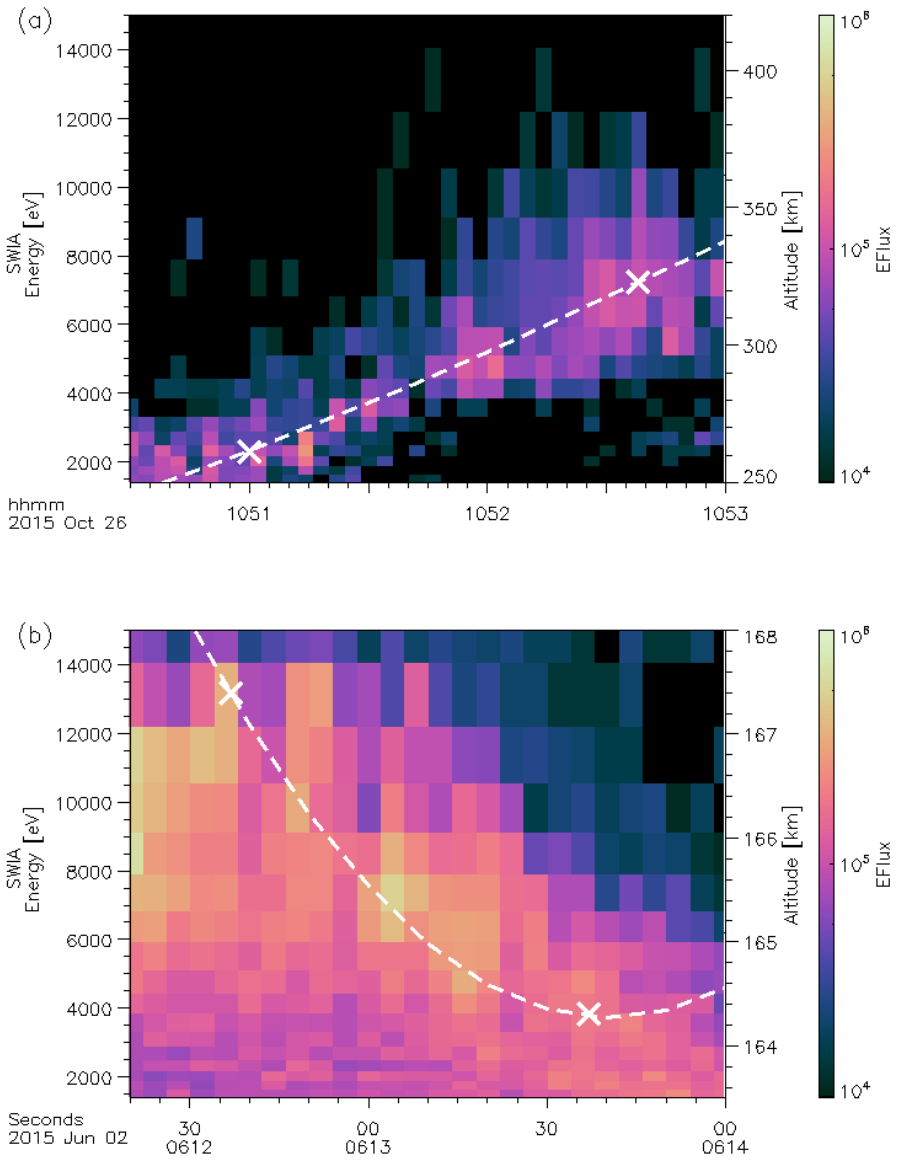

Figure 9. Examples of energy dispersed keV ions that mark the transition between keV ion bands features and the appearance of (a) broad energy range ion spike 2 observed on October 26th, 2015 and (b) broad energy range ion spike 5 observed on June 2nd, 2015. Dashed lines demonstrate the linear dependence of ion energy with altitude and cross marks show the limits used for determining an electric field strength associated with the deceleration of the ions.

©2018 American Geophysical Union. All rights reserved.

Accepted Article

7 Energy deposition from precipitating ions in radial crustal magnetic fields

Occurring at low altitudes, below 300 km, the keV ion precipitation observed during ion spikes studied here on the dayside of Mars may present important periods of energy deposition, although episodic and localized. In comparison to solar EUV energy absorbed below 300 km on the dayside by the Martian atmosphere, contributions from electron precipitation and energy from electromagnetic waves are negligible. Energy from electromagnetic waves may play an important role in the outflow of ions in regions of collisionless plasma at higher altitudes [*Ergun et al.*, 2006], whereas electron precipitation is the dominant source of energy input into the nightside Martian atmosphere [*Lillis et al.*, 2015; *Fillingim et al.*, 2010]. Modeling by *Fang et al.* [2013] shows that pick-up O^+ ions precipitating towards Mars from the -E hemisphere of the Mars-Sun-Electric field (MSE) frame can result in significant energy deposition on the dayside of Mars compared to input from solar EUV energy, varying between negligible to very important effects on the thermosphere when upstream solar wind conditions vary from normal to extreme.

In the case of the ion precipitation from ion spike 2 presented in Fig. 5, the energy deposition between 1.3 keV - 7.5 keV from the accelerated beam of O^+ ions in energy flux is calculated by integrating SWIA energy flux measurements over the energy and solid angle corresponding to the observation of the ion beam and results in 5.5×10^{-7} W/m^2 (3.5×10^8 eV/(cm^2.sec)). The mass deposition in number flux is calculated by integrating SWIA flux measurements over the energy and solid angle corresponding to the observation of the ion beam and results in 1.4×10^5 #/(cm^2.sec). In the case of the ion precipitation presented in Fig. 6, the energy deposition between 1.3 keV - 9.0 keV from the accelerated ion beam, assumed as O^+ ions, in energy flux is 3.6×10^{-6} W/m^2 (2.3×10^9 eV/(cm^2.sec)) and mass deposition in number flux is 7.1×10^5 #/(cm^2.sec). This compares to the average SWIA ion precipitating flux for radial magnetic field orientations from the study by *Hara et al.* [2018], resulting in an energy deposition between 1.3 keV - 9.0 keV for energy flux over a 70° precipitating cone angle, 2.9×10^{-6} W/m^2 (1.8×10^9 eV/(cm^2.sec)) and mass deposition in number flux, 5.3×10^5 #/(cm^2.sec).

The most significant effect from ion precipitation on the dayside of Mars may be from momentum transfer during ion-neutral collisions where a sputtering process can result in the escape of atmosphere [*Luhmann and Kozyra*, 1991; *Johnson et al.*, 2000; *Leblanc and Johnson*, 2001]. Relationships derived by *Wang et al.* [2015] from the mod-

©2018 American Geophysical Union. All rights reserved.

Accepted Article

eling of O^+ sputtering effects can be applied to MAVEN observations to estimate possible escape rates. Using the values for precipitating energy flux and number flux determined from Fig. 5 in equation 14 from *Wang et al.* [2015] results in an escape rate of 6.0×10^4 /(cm^2.sec) for precipitation of the accelerated ion beam from 1.4 keV - 7.5 keV and 9.0×10^4 /(cm^2.sec) for the broader precipitation of ions between 25 eV - 0.1 keV. Using the sputtering yield tables for O given by Figure A1 from *Wang et al.* [2015], a maximum yield of ~450% for precipitating 1.4 keV - 7.5 keV O^+ ions with incident angles of 0° - 20° results in an escape of 6.3×10^5 /(cm^2.sec), and a maximum sputtering yield of ~100% for precipitating 25 eV - 0.1 keV O^+ ions with incident angles of 0° - 45° results in an escape of 1.5×10^6 /(cm^2.sec).

8 Summary and conclusions

For the first time at Mars, simultaneous ion, electron, magnetic field vector and electric field wave measurements from the MAVEN PFP instrument suite have been used to study the plasma transport processes and associated electrodynamic effects related to broad energy range ion spikes of ion energy flux in regions of the low altitude (>300 km) radial crustal magnetic field, aka cusps, on the dayside of Mars. This also allows the unambiguous characterization for the kinetic behavior of ions from ion velocity distributions formed with use of in-situ vector measurements of the magnetic field, which has not been achieved before at Mars from measurements in the low altitude crustal magnetic fields. Time periods have been chosen that show the extraordinary coincidence of signatures of energy flux ion spikes observed in radial crustal magnetic fields and energy-time bands of keV ions that extend over horizontal crustal magnetic fields.

The ion spikes are characterized by the precipitation towards Mars of different ion populations; planetary-like O^+ and O_2^+ ions and magnetosheath-like H^+ ions and when coinciding with keV ion energy-time bands also involved keV O^+ ions typical of ions picked-up by the solar wind. The ion spikes presented here are also observed alongside the precipitation of energetic electrons or electron spikes in energy flux along radial magnetic field lines that have been assumed as being closed.

Populations of H^+ ion E<1.4 keV and O^+ and O_2^+ ions E<0.1 keV are observed with broad ion velocity distributions precipitating towards Mars and are interpreted as ions flowing from higher altitude crustal magnetic fields. This may occur as a result of the in-

©2018 American Geophysical Union. All rights reserved.

Accepted Article

jection of ions following either magnetic reconnection or a filling of the loss cone by the pitch angle scattering from non-adiabatic effects or wave particle interactions.

Depending on ion energy (H^+ E>320 eV) or mass (O^+ and O_2^+ E<0.1 keV), ion velocity distributions measured during the spikes show ions precipitating from above can have non-adiabatic characteristics possibly retained after been transported from regions of weaker magnetic field. Also, at the same time a reflected component of ions and a loss cone is observed for ions moving away from Mars and this is indicative of the conservation of first adiabatic invariant in a mirror field for ions transported from lower altitudes. This is further exemplified by observations around ~175 km altitude of non-gyrotropic partial ring distributions of H^+ ions precipitating towards Mars. Distributions of mirroring ions may be unstable to plasma waves and perpendicular ion heating. This is supported by the first tentative observations of ion conics directed away from Mars in radial crustal magnetic fields. Considering only the effects of a charge exchange process on a mirroring population of precipitating H^+ ions, could result in an additional hydrogen escape from Mars if the original source of the precipitating H^+ ions is from the hot ion corona of Mars instead of the solar wind. Evidence of the adiabatic behavior of ions is observed in spite of the parameter of adiabaticity from the expected radius of curvature of the crustal magnetic field not supporting adiabatic effects. This would suggest ions are injected with highly field aligned distributions at higher altitudes or that the crustal magnetic fields have a radius of curvature that is much larger than expected.

The precipitating ion and electron spikes also occur alongside remarkably large perturbations in the background magnetic field, with magnitudes of up to 60 nT and large wave amplitudes in the electric field. These large electric field wave amplitudes are measured at perpendicular to oblique angles to the local magnetic field and occur over short time scales, typically between 1 mV/m - 10 mV/m and with large outliers between 20 mV/m - 38 mV/m. Greater fluctuations in the electric field in regions of the crustal magnetic field cusps are associated with LPW measurements deviating slightly from angles perpendicular to the magnetic field, as well as ion velocity distributions that showed a combination of non-gyrotropic partial ring distributions of H^+ ions with features suggestive of a transverse heating / energization of ions precipitating towards Mars and ions moving away from Mars at conical angles to the magnetic field.

©2018 American Geophysical Union. All rights reserved.

Accepted Article

The measurement of fluctuating electric fields with perpendicular to oblique angles to the magnetic field could translate to small scale double layer structures and a series of small scale field aligned electric fields or potential drops. Indeed, brief observations of field aligned peaked electrons up to energies of 150 eV precipitating towards Mars would support the possibility of a small scale DC accelerating fields. It is proposed that the presence of large electric fields measured in the radial crustal magnetic field regions could be supported by a charge separation dynamo as caused by the different altitudes observed for reflected electrons and ions and mirroring of H^+ ions around ~175 km.

The precipitating ions >1.4 keV, as associated with O^+ ions, occur as accelerated ion beams as would occur due to the injection of ions accelerated externally, but are also observed as field aligned ions that have been heated by a more local process. Although, it is not known if the heating is caused by the energization or deceleration of ions. Energy dispersed structures of O^+ ions that could signify the deceleration of ions by electric fields as large as ~3 V/m in the radial extent and ~40 mV/m along the MAVEN orbit path, are instead interpreted as a velocity selection effect of pick-up ions over radial crustal magnetic field. That is ions picked-up at closer distances to Mars that are of lower energy have more Marsward (field aligned) trajectories and are preferentially selected in regions of radial crustal magnetic fields. This compares to ions picked-up at further distances that are of higher energy, which have more anti-Sunward trajectories and will experience greater reflection in regions of radial crustal magnetic fields and also as the strength of the magnetic field increases in such regions.

The precipitating O^+ ions observed during the ion spikes reported here will have implications for sputtering and localized atmospheric heating, with the calculation of energy deposition rates as large as 3.6×10^{-6} W/m^2 and mass deposition rates as large as of 7.1×10^5 #/cm^2.sec. The total sputtering escape rates of 1.5×10^5 /(cm^2.sec) and 2.1×10^6 /(cm^2.sec) are calculated using the sputtering response relation and O sputtering yield tables from *Wang et al.* [2015] respectively. Considering ion spike 2 is observed over an expanse of 0.7° latitude at an altitude of around 260 km, that is a flux tube of around 22 km radius with a cross sectional area of roughly 1.5×10^3 km^2, this could relate to a total mass loss of O atoms of ~6×10^{-8} kg/s (~5×10^{-3} kg/day), as derived from sputtering response relations and ~8×10^{-7} kg/s (~70×10^{-3} kg/day), as derived from sputtering yield tables from *Wang et al.* [2015].

©2018 American Geophysical Union. All rights reserved.

Accepted Article

Acknowledgments

The MAVEN mission is supported by NASA through the Mars Scout program. All data presented as part of this paper are available on the Planetary Data System (https://pds-ppi.igpp.ucla.edu/search/?sc=MAVEN).

References

Acuña, M., et al. (1998), Magnetic field and plasma observations at Mars: Initial results of the Mars Global Surveyor mission, *Science*, 279, 1676-1680, doi:10.1126/science.279.5357.1676.

Alem, F., and D. C. Delcourt (1995), Nonadiabatic precipitation of ions at the cusp equatorward edge, *J. Geophys. Res.*, 100(A10), 19321-19328, doi:10.1029/95JA01160.

Andersson, L., R. E. Ergun, G. T. Delory, A. Eriksson, J. Westfall, H. Reed, J. McCauly, D. Summers and D. Meyers (2015). The Langmuir Probe and Waves (LPW) Instrument for MAVEN, *Space Sci. Rev.*, 195, 173-198, doi:10.1007/s11214-015-0194-3.

André, M. and A., Yau (1997), Theories and observations of ion energization and outflow in the high latitude magnetosphere, *Space Sci. Rev.*, 80, 27-48, doi:10.1023/A:1004921619885.

Bertaux, J.-L., F. Leblanc, O. Witasse, E. Quemerais, J. Lilensten, S. A. Stern, B. Sandel and O. Korablev (2005), Discovery of an aurora on Mars, *Nature*, 435, 790-794, doi:10.1038/nature03603.

Block L.P. (1988) Acceleration of auroral particles by magnetic-field aligned electric fields, *Astrophys. Space Sci.*, 144, 135-147, doi:10.1007/BF00793177.

Bouhram, M., N. Dubouloz, M. Malingre, J. R. Jasperse, R. Pottelette, C. Senior, D. Delcourt, C. W. Carlson, I. Roth, M. Berthomier, and J. A. Sauvaud (2002), Ion outflow and associated perpendicular heating in the cusp observed by Interball Auroral Probe and Fast Auroral Snapshot, *J. Geophys. Res.*, 107(A2), doi:10.1029/2001JA000091.

Brain, D. A., Halekas, J. S., Lillis, R. J., Mitchell, D. L., Lin, R. P. and Crider, D. H. (2005), Variability of the altitude of the Martian sheath. *Geophys. Res. Lett.*, 32, L18203. doi:10.1029/2005GL023126

Brain, D. A., et al. (2006), On the origin of aurorae on Mars, *Geophys. Res. Lett.*, 33, L01201, doi:10.1029/2005GL024782.

Brain, D. A., R. J. Lillis, D. L. Mitchell, J. S. Halekas and R. P. Lin (2007), Electron pitch angle distributions as indicators of magnetic field topology near Mars, *J. Geophys.*

©2018 American Geophysical Union. All rights reserved.

Res., 112, A09201, doi:10.1029/2007JA012435.

Brain, D. A., J. S. Halekas, L. M. Peticolas, R. P. Lin, J. G. Luhmann, D. L. Mitchell, G. T. Delory, S. W. Bougher, M. H. Acuña and H. Rème (2010), On the origin of aurorae on Mars, *Geophys. Res. Lett.*, 33, L01201, doi:10.1029/2005GL024782.

Brecht, S. H. and S. A. Ledvina (2012), Control of ion loss from Mars during solar minimum, *Earth, Planets and Space*, 64, 165-178, doi:10.5047/eps.2011.05.037.

Briggs, J.A., D. A. Brain, M. L. Cartwright, J. P. Eastwood and J. S. Halekas (2011), A statistical study of flux ropes in the martian magnetosphere. *Planet Space Sci.*, 59, 1498-1505, doi:10.1016/j.pss.2011.06.010.

Buchner, J., and L. M. Zelenyi (1986), Deterministic chaos in the dynamics of charged particles near a magnetic field reversal, *Phys. Lett. A*, 118, 395, doi:10.1016/0375-9601(86)90268-9.

Buchner, J., and L. M. Zelenyi (1989), Regular and chaotic charged particle motion in magnetotail-like field reversals: 1. Basic theory of trapped motion, *J. Geophys. Res.*, 94, 11,821, doi:10.1029/JA094iA09p11821.

Cattell, C. and Hudson, M. (1982), Flute mode waves near the lower hybrid frequency excited by ion rings in velocity space. *Geophys. Res. Lett.*, 9, 1167-1170, doi:10.1029/GL009i010p01167.

Cole, K. D., Effects of crossed magnetic and (spatially dependent) electric fields on charged particle motion, *Planet. Space Sci.*, 24, 515-518., doi:10.1016/0032-0633(76)90096-9.

Collinson, G., et al. (2015), ElectricMars: The first direct measurement of an upper limit for the Martian "polar wind" electric potential, *Geophys. Res. Lett.*, 42, 9128-9134, doi:10.1002/2015GL065084.

Connerney, J. E. P. , M. H. Acuña, P. J. Wasilewski, G. Kletetschka, N. F. Ness, H. Rème, R. P. Lin and D. L. Mitchell (2001), The Global Magnetic Field of Mars and Implications for Crustal Evolution, *Geophys. Res. Lett.*, 28, 4015-4018, doi:10.1029/2001GL013619.

Connerney, J. E. P., M. H. Acuña, N. F. Ness, G. Kletetschka, D. Mitchell, R. P. Lin and H. Reme (2005), Tectonic implications of Mars crustal magnetism, *Proc. Nat. Acad. Sci.*, 102, (42), 14970-14975, doi:10.1073/pnas.0507469102.

Connerney, J. E. P., J. R. Espley, P. Lawton, S. Murphy, J. Odom, R. Oliversen and D. Sheppard (2015a), The MAVEN Magnetic Field Investigation, *Space Sci. Rev.*, 195, 257-

©2018 American Geophysical Union. All rights reserved.

Accepted Article

291, doi:10.1007/s11214-015-0169-4.

Connerney, J.E.P., J.R. Espley, G.A. DiBraccio, J.R. Gruesbeck, R.J. Oliversen, D. L. Mitchell, J. Halekas, C. Mazelle, D.A. Brain and B. M. Jakosky (2015b), First results of the MAVEN magnetic field investigation, *Geophys. Res. Lett.*, 42, 8819-8827, doi:10.1002/2015GL065366.

Curry, S. M., J. Luhmann, M. J. Yingjuan, L. Michael, C. Dong and T. Hara (2015), Comparative pick-up ion distributions at Mars and Venus: Consequences for atmospheric deposition and escape, *Planet. Space Sci.*, 115, 35-47, doi:10.1016/j.pss.2015.03.026.

Deca, J., A. Divin, B. Lembège, M. Horányi, S. Markidis, and G. Lapenta (2015), General mechanism and dynamics of the solar wind interaction with lunar magnetic anomalies from 3-D particle-in-cell simulations, *J. Geophys. Res. Space Physics*, 120, 6443-6463, doi:10.1002/2015JA021070.

Dong, C., S. W. Bougher, Y. Ma, G. Toth, Y. Lee, A. F. Nagy, V. Tenishev, D. J. Pawlowski, M. R. Combi, and D. Najib (2015), Solar wind interaction with the Martian upper atmosphere: Crustal field orientation, solar cycle, and seasonal variations, *J. Geophys. Res. Space Physics*, 120, 7857-7872, doi:10.1002/2015JA020990.

Dubinin, E., R. Lundin, O. Norberg and N. Pissarenko (1993), Ion acceleration in the Martian tail: Phobos observations, *J. Geophys. Res.*, 98, 3991-3997, doi:10.1029/92JA02233.

Dubinin, E., R. Lundin, and K. Schwingenschuh (1994), Solar wind electrons as tracers of the Martian magnetotail topology, *J. Geophys. Res.*, 99(A11), 21233-21240, doi: 10.1029/94JA01271.

Dubinin, E., et al. (2006a), Electric fields within the martian magnetosphere and ion extraction: ASPERA-3 observations, *Icarus*, 182, 337-342, doi:10.1016/j.icarus.2005.05.022.

Dubinin, E., M. Fraenz, J. Woch, S. Barabash, R. Lundin and M. Yamauchi (2006b), Hydrogen exosphere at Mars: Pickup protons and their acceleration at the bow shock, *Geophys. Res. Lett.*, 33, L22103, doi:10.1029/2006GL027799.

Dubinin, E., G. Chanteur, M. Fraenz, J. Woch (2008), Field-aligned currents and parallel electric field potential drops at Mars. Scaling from the Earth? aurora, *Planet. Space Sci.*, 56, 868-872, doi:10.1016/j.pss.2007.01.019.

©2018 American Geophysical Union. All rights reserved.

Accepted Article

Accepted Article

Dubinin, E., M. Fraenz, J. Woch, S. Barabash, and R. Lundin (2009), Long-lived auroral structures and atmospheric losses through auroral flux tubes on Mars, *Geophys. Res. Lett.*, 36, L08108, doi:10.1029/2009GL038209.

Dubinin, E., M. Fraenz, A. Fedorov, R. Lundin, N. Edberg, F. Duru and O. Vaisberg (2011), Ion Energization and Escape on Mars and Venus, *Space Sci Rev*, 162, 173-211, doi:10.1007/s11214-011-9831-7.

Ergun, R. E., L. Andersson, W. K. Peterson, D. Brain, G. T. Delory, D. L. Mitchell, R. P. Lin, and A. W. Yau (2006), Role of plasma waves in Mars' atmospheric loss, *Geophys. Res. Lett.*, 33, L14103, doi:10.1029/2006GL025785.

Fang, X., M. W. Liemohn, A. F. Nagy, J. G. Luhmann, Y. Ma (2010), On the effect of the martian crustal magnetic field on atmospheric erosion, *Icarus*, 206, 130-138, doi:10.1016/j.icarus.2009.01.012.

Fang, X., S. W. Bougher, R. E. Johnson, J. G. Luhmann, Y. Ma, Y.-C. Wang, and M. W. Liemohn (2013), The importance of pickup oxygen ion precipitation to the Mars upper atmosphere under extreme solar wind conditions, *Geophys. Res. Lett.*, 40, 1922-1927, doi:10.1002/grl.50415.

Fang, X., Y. Ma, D. Brain, Y. Dong, and R. Lillis (2015), Control of Mars global atmospheric loss by the continuous rotation of the crustal magnetic field: A time-dependent MHD study, *J. Geophys. Res. Space Physics*, 120, 10,926-10,944, doi:10.1002/201

Fillingim, M. O., L. M. Peticolas, R. J. Lillis, D. A. Brain, J. S. Halekas, D. Lummerzheim, and S. W. Bougher (2010), Localized ionization patches in the nighttime ionosphere of Mars and their electrodynamic consequences, *Icarus*, 206, 112-119, doi:10.1016/j.icarus.2009.03.005.

Fowler, C. M., L. Andersson, J. Halekas, J. R. Espley, C. Mazelle, E. R. Coughlin, R. E. Ergun, D. J. Andrews, J. E. P. Connerney, and B. Jakosky (2017), Electric and magnetic variations in the near-Mars environment, *J. Geophys. Res. Space Physics*, 122, 8536-8559, doi:10.1002/2016JA023411.

Frahm, R. A., et al. (2006), Carbon dioxide photoelectron energy peaks at Mars, *Icarus*, 182, 371-382, doi:10.1016/j.icarus.2006.01.014.

Fränz, M., et al. (2006), Plasma intrusion above Mars crustal fields - Mars Express ASPERA-3 observations, *Icarus* 182, 406-412, doi:10.1016/j.icarus.2005.11.016.

Fränz, M., E. Dubinin, E. Nielsen, J. Woch, S. Barabash, R. Lundin and A. Fedorov (2010). Transterminator ion flow in the Martian ionosphere, *Planet. Space Sci.*, 58,

©2018 American Geophysical Union. All rights reserved.

1442-1454, doi:10.1016/j.pss.2010.06.009.

Futaana, Y., S. Barabash, M. Wieser, C. Lue, P. Wurz, A. Vorburger, A. Bhardwaj and K. Asamura (2013), Remote energetic neutral atom imaging of electric potential over a lunar magnetic anomaly, *Geophys. Res. Lett.*, 40, 262-266, doi:10.1002/grl.50135.

Gérard, J.-C., L. Soret, L. Libert, R. Lundin, A. Stiepen, A. Radioti, and J.-L. Bertaux (2015), Concurrent observations of ultraviolet aurora and energetic electron precipitation with Mars Express, *J. Geophys. Res. Space Physics*, 120, 6749-6765, doi:10.1002/2015JA021150.

Giacalone, J., and L. L. Hood (2015), Hybrid simulation of the interaction of solar wind protons with a concentrated lunar magnetic anomaly, *J. Geophys. Res. Space Physics*, 120, 4081-4094, doi:10.1002/2014JA020938.

Gorney, D. J. (1983), An alternative interpretation of ion ring distributions observed by the S3-3 satellite, *Geophys. Res. Lett.*, 10, 417-420, doi:10.1029/GL010i005p00417.

Grigorenko, E. E., M. Hoshino, M. Hirai, T. Mukai, and L. M. Zelenyi (2009), "Geography" of ion acceleration in the magnetotail: X-line versus current sheet effects, *J. Geophys. Res.*, 114, A03203, doi:10.1029/2008JA013811.

Hara, T., et al. (2017a), MAVEN observations of a giant ionospheric flux rope near Mars resulting from interaction between the crustal and interplanetary draped magnetic fields, *J. Geophys. Res. Space Physics*, 122, 828-842, doi:10.1002/2016JA023347.

Hara, T., et al. (2017b), MAVEN observations on a hemispheric asymmetry of precipitating ions toward the Martian upper atmosphere according to the upstream solar wind electric field, *J. Geophys. Res. Space Physics*, 122, 1083-1101, doi:10.1002/2016JA023348.

Hara, T., et al. (2018), Evidence for crustal magnetic field control of ions precipitating into the upper atmosphere of Mars, *J. Geophys. Res.*, 122, doi:10.1029/2017JA024798.

Harada, Y., et al. (2015), Magnetic reconnection in the near-Mars magnetotail: MAVEN observations, *Geophys. Res. Lett.*, 42, 8838-8845, doi:10.1002/2015GL065004.

Harada, Y., et al. (2016), MAVEN observations of energy-time dispersed electron signatures in Martian crustal magnetic fields, *Geophys. Res. Lett.*, 43, 939-944, doi:10.1002/2015GL067040.

Halekas, J. S., D. A. Brain, R. P. Lin, J. G. Luhmann and D. L. Mitchell (2008), Distribution and variability of accelerated electrons at Mars, *Adv. Space. Res.*, 195, 125-151, doi:10.1016/j.asr.2007.01.

©2018 American Geophysical Union. All rights reserved.

Accepted Article

Halekas, J. S., et al. (2015a), The Solar Wind Ion Analyzer for MAVEN, *Space Sci. Rev.*, 41, 1347-1352, doi:10.1007/s11214-013-0029-z.

Halekas, J. S., et al. (2015b), MAVEN observations of solar wind hydrogen deposition in the atmosphere of Mars, *Geophys. Res. Lett.*, 42, 8901-8909, doi:10.1002/2015GL064693.

Hudson, M. K. and Roth, I. (1986), Ion Heating in the Cusp, in Ion Acceleration in the Magnetosphere and Ionosphere (eds T. Chang, M. K. Hudson, J. R. Jasperse, R. G. Johnson, P. M. Kintner and M. Schulz), American Geophysical Union, Washington, D. C.. doi: 10.1029/GM038p0271.

Jakosky, B. M., Lin, R. P., Grebowsky, J. M., et al. (2015), The Mars Atmosphere and Volatile Evolution (MAVEN) Mission, *Space Sci. Rev.*, 195, 3-48, doi:10.1007/s11214-015-0139-x.

Kallio, E., A. Fedorov, E. Budnik, S. Barabash, R. Jarvinen and P. Janhunen (2008), On the properties of O^+ and O_2^+ ions in a hybrid model and in Mars Express IMA/ASPERA-3 data: A case study, *Planet. Space Sci.*, 1204-1213, doi:10.1016/j.pss.2008.03.007.

Kallio, E. et al. (2012), Kinetic simulations of finite gyroradius effects in the lunar plasma environment on global, meso, and microscales, *Planet. Space Sci.*, 74, 146-155, doi:10.1016/j.pss.2012.09.012.

Knudsen, W., K. Spenner and K. Miller (1981), Anti-solar acceleration of ionospheric plasma across the Venus terminator, *Geophys. Res. Lett.*, 8, 241-244, doi:10.1029/GL008i003p00241.

Johnson, R. E., D. Schnellenberger, and M. C. Wong (2000), The sputtering of an oxygen thermosphere by energetic O^+, *J. Geophys. Res.*, 105(E1), 1659-1670, doi:10.1029/1999JE001058.

Leblanc, F. and R. E. Johnson (2001). Sputtering of the Martian atmosphere by solar wind pick-up ions, *Planet. Space Sci.*, 49, 645-656, doi:10.1016/j.pss.2015.03.026.

Leblanc, F. and R. E. Johnson (2002). Role of molecular species in pickup ion sputtering of the Martian atmosphere, *J. Geophys. Res.*, 107(E2), doi:10.1029/2000JE001473.

Li, L., Y. Zhang, Y. Feng, X. Fang and Y. Ma (2011), Oxygen ion precipitation in the Martian atmosphere and its relation with the crustal magnetic fields, *J. Geophys. Res.*, 116, A08204, doi:10.1029/2010JA016249.

©2018 American Geophysical Union. All rights reserved.

Accepted Article

Lillis, R. J., and X. Fang (2015), Electron impact ionization in the Martian atmosphere: Interplay between scattering and crustal magnetic field effects, *J. Geophys. Res. Planets*, 120, doi:10.1002/2015JE004841.

Lillis, R. J., Halekas, J. S., Fillingim, M. O., Poppe, A. R., Collinson, G., Brain, D. A. and Mitchell, D. L. (2018), Field-aligned electrostatic potentials above the Martian exobase from MGS electron reflectometry: Structure and variability, *J. Geophys. Res. Planets*, 123, 67-92. https://doi.org/10.1002/2017JE005395.

Lindstedt, T., Y. V. Khotyaintsev, A. Vaivads, M. André, H. Nilsson, and M. Waara (2010), Oxygen energization by localized perpendicular electric fields at the cusp boundary, *Geophys. Res. Lett.*, 37, L09103, doi: 10.1029/2010GL043117.

Lundin, R., et al. (2006a), Plasma Acceleration Above Martian Magnetic Anomalies, *Science*, 311, 980, doi:10.1126/science.1122071.

Lundin, R., Winningham, D., Barabash, S. et al. (2006b), Auroral Plasma Acceleration Above Martian Magnetic Anomalies, *Space Sci. Rev.*, 126, 333-354, doi:10.1007/s11214-006-9086-x.

Lundin, R., S. Barabash, M. Yamauchi, H. Nilsson, and D. Brain (2011), On the relation between plasma escape and the Martian crustal magnetic field, *Geophys. Res. Lett.*, 38, L02102, doi:10.1029/2010GL046019.

Luhmann, J. G., and J. U. Kozyra (1991), Dayside pickup oxygen ion precipitation at Venus and Mars: Spatial distributions, energy deposition and consequences, *J. Geophys. Res.*, 96(A4), 5457-5467, doi:10.1029/90JA01753.

Ma, Y., X. Fang, C. T. Russell, A. F. Nagy, G. Toth, J. G. Luhmann, D. A. Brain and C. Dong (2014), Effects of crustal field rotation on the solar wind plasma interaction with Mars, *Geophys. Res. Lett.*, 41, 6563-6569, doi:10.1002/ 2014GL060785.

Mahaffy, P. R., M. Benna, T. King et al. (2015a), The Neutral Gas and Ion Mass Spectrometer on the Mars Atmosphere and Volatile Evolution Mission, *Space Sci. Rev.*, 195, 49-73, doi:10.1007/s11214-014-0091-1.

Mahaffy, P. R., M. Benna, M. Elrod, R. V. Yelle, S. W. Bougher, S. W. Stone,and B. M. Jakosky (2015b), Structure and composition of the neutral upper atmosphere of Mars from the MAVEN NGIMS investigation, *Geophys. Res. Lett.*, 42, 8951-8957, doi:10.1002/2015GL065329.

Martin, R. F., D. Delcourt, D. L. Holland and M. J. Asbury (2000), Magnetotail particle distributions associated with pitch angle isotropization, *J. Atmospheric Sol.-Terr. Phys.*,

©2018 American Geophysical Union. All rights reserved.

Accepted Article

62, 513-519, doi:10.1016/S1364-6826(00)00020-1.

McFadden, J. P., et al. (2015), MAVEN SupraThermal and Thermal Ion Compostion (STATIC) Instrument, *Space Sci. Rev.*, 195, 199-256, doi:10.1007/s11214-015-0175-6.

Mitchell, D. L., R. P. Lin, C. Mazelle, H. Rème, P. A. Cloutier, J. E. P. Connerney, M. H. Acuña and N. F. Ness (2001), Probing Mars' crustal magnetic field and ionosphere with the MGS Electron Reflectometer, *J. Geophys. Res.*, 106 (El0), 23419-23427, doi:10.1029/2000JE001435.

Mitchell, D. L., et al. (2016), The MAVEN Solar Wind Electron Analyzer, *Space Sci. Rev.*, 200, 495-528, doi:10.1007/s11214-015-0232-1.

Morschhauser, A., V. Lesur, and M. Grott (2014). A spherical harmonic model of the lithospheric magnetic field of Mars, *J. Geophys. Res. Planets*, 119, 1162–1188, doi:10.1002/2013JE004555.

Nagy, A. F., D. Winterhalter, K. Sauer, T. E. Cravens, S. Brecht, C. Mazelle, D. Crider, E. Kallio, A. Zakharov, E. Dubinin, M. Verigin, G. Kotova, W. I. Axford, C. Bertucci and J. G. Trotignon (2004). The plasma Environment of Mars, *Space Sci. Rev.*, 111, 33-114, doi:10.1023/B:SPAC.0000032718.47512.92.

Nielsen, E., et al. (2007), Local plasma processes and enhanced electron densities in the lower ionosphere in magnetic cusp regions on Mars, *Planet. Space Sci.*, 55, 2164-2172, doi:10.1016/j.pss.2007.07.003.

Nilsson, H., N. J.T. Edberg, G. Stenberg, S. Barabash, M. Holmström, Y. Futaana, R. Lundin, A. Fedorov (2011), Heavy ion escape from Mars, influence from solar wind conditions and crustal magnetic fields, *Icarus*, 215, 475-484, doi:10.1016/j.icarus.2011.08.003.

Poppe, A R., S. Fatemi, I. Garrick-Bethell, D. Hemingway and M. Holmström (2016), Solar wind interaction with the Reiner Gamma crustal magnetic anomaly: Connecting source magnetization to surface weathering, *Icarus*, 266, 261-266, doi:10.1016/j.icarus.2015.11.005.

Opgenoorth, H. J., R. S. Dhillon, L. Rosenqvist, M. Lester, N. J. T. Edberg, S. E. Milan, P. Withers and D. Brain (2010). Day-side ionospheric conductivities at Mars, *Planet. Space Sci.*, 58, 1139-1151, doi:10.1016/j.pss.2010.04.004.

Øieroset, M., M. Yamauchi, L. Liszka, and B. Hultqvist (1999), Energetic ion outflow from the dayside ionosphere: Categorization, classification, and statistical study, *J. Geophys. Res.*, 104(A11), 24915-24927, doi:10.1029/1999JA900248.

©2018 American Geophysical Union. All rights reserved.

Accepted Article

Onsager, T. G., C. A. Kletzing, J. B. Austin and H. MacKiernan (1993), Model of magnetosheath plasma in the magnetosphere: Cusp and mantle particles at low-altitudes, *Geophys. Res. Lett.*, 20, 479-482, doi:10.1029/93GL00596.

Rahmati, A., D. E. Larson, T. E. Cravens, R. J. Lillis, P. A. Dunn, J. S. Halekas, J. E. Connerney, F. G. Eparvier, E. M. B. Thiemann, and B. M. Jakosky (2015), MAVEN insights into oxygen pickup ions at Mars, *Geophys. Res. Lett.*, 42, 8870-8876, doi:10.1002/2015GL065262.

Raines, J. M., D. J. Gershman, J. A. Slavin, T. H. Zurbuchen, H. Korth, B. J. Anderson, and S. C. Solomon (2014), Structure and dynamics of Mercury's magnetospheric cusp: MESSENGER measurements of protons and planetary ions, *J. Geophys. Res. Space Physics*, 119, 6587-6602, doi:10.1002/2014JA020120.

Ramstad, R., S. Barabash, Y. Futaana, H. Nilsson, and M. Holmström (2016), Effects of the crustal magnetic fields on the Martian atmospheric ion escape rate, *Geophys. Res. Lett.*, 43, 10,574-10,579, doi:10.1002/2016GL070135.

Roelof, E.C (1997) ENA emission from nearly-mirroring magnetospheric ions interacting with the exosphere, *Adv. Space Res.*, 20, 361-366, doi:10.1016/S0273-1177(97)00692-3.

Roth, I., and M. K. Hudson (1985), Lower hybrid heating of ionospheric ions due to ion ring distributions in the cusp, *J. Geophys. Res.*, 90(A5), 4191-4203, doi:10.1029/JA090iA05p04191.

Saito, Y. et al. (2012), Simultaneous observation of the electron acceleration and ion deceleration over lunar magnetic anomalies, *Earth Planet Sp.*, 64, 83-91, doi:10.5047/eps.2011.07.011.

Soobiah, Y. I. J., et al. (2006), Observations of magnetic anomaly signatures in Mars Express ASPERA-3 ELS data, *Icarus*, 182, 396-405, doi:10.1016/j.icarus.2005.10.034.

Soobiah, Y. I. J., S. Barabash, H. Nilsson, G. Stenberg, R. Lundin, A.J. Coates, J.D. Winningham and R.A. Frahm (2013), Energy distribution asymmetry of electron precipitation signatures at Mars, *Planet. Space Sci.*, 76, 10-27, doi:10.1016/j.pss.2012.10.014.

Soobiah, Y. I. J., J. A. Wild, M. J. Beharrell, S. Barabash, R. J. Lillis, D. L. Mitchell, A. J. Coates, J. D. Winningham and R. A. Frahm (2014), Properties of a large-scale flux rope and current sheet region on the dayside of Mars: MGS MAG/ER and MEX ASPERA-3 ELS observations, *Icarus*, 242, 297-315, doi:10.1016/j.icarus.2014.08.019.

O. Vaisberg (2015), Mars atmospheric losses induced by the solar wind: Comparison of observations with models, *Planet. Space Sci.*, 119, 69-91 doi:10.1016/j.pss.2015.09.007.

©2018 American Geophysical Union. All rights reserved.

Accepted Article

Vaisberg, O., A. Artemyev and L. Avanov (2015), Nonadiabatic ion acceleration at the nightside highlatitude magnetopause: Fine structure of the velocity distribution function, *Adv. Space Res.*, 55, 2840-2850, doi:10.1016/j.asr.2015.02.036.

Wang, X.-D., S. Barabash, Y. Futaana, A. Grigoriev, and P. Wurz (2014), Influence of Martian crustal magnetic anomalies on the emission of energetic neutral hydrogen atoms, *J. Geophys. Res. Space Physics*, 119, 8600-8609, doi:10.1002/2014JA020307.

Wang, Y.-C., J. G. Luhmann, X. Fang, F. Leblanc, R. E. Johnson, Y. Ma, and W.-H. Ip (2015), Statistical studies on Mars atmospheric sputtering by precipitating pickup O^+: Preparation for the MAVEN mission, *J. Geophys. Res. Planets*, 120, 34-50, doi:10.1002/2014JE004660.

Xu, S., et al. (2017), Martian low-altitude magnetic topology deduced from MAVEN/SWEA observations, *J. Geophys. Res. Space Physics*, 122, doi:10.1002/ 2016JA023467.

Yamauchi, M. et al. (2006), IMF direction derivation from cycloid-like ion distributions observed by Mars Express, *Space Sci. Rev.*, 126 (1?4), 239?266, doi:10.1007/s11214-006-9090-1.

Yamauchi, M., Y. Futaana, A. Fedorov, E. Kallio, R. A. Frahm, R. Lundin, J.- A. Sauvaud, D.J. Winningham, S. Barabash and M. Holmström (2008), Advanced method to derive the IMF direction near Mars from cycloidal proton distributions, *Planet. Space Sci.*, 56 (8), 1145?1154, doi:10.1016/j.pss.2008.02.012.

©2018 American Geophysical Union. All rights reserved.

Accepted Article

Accepted Article

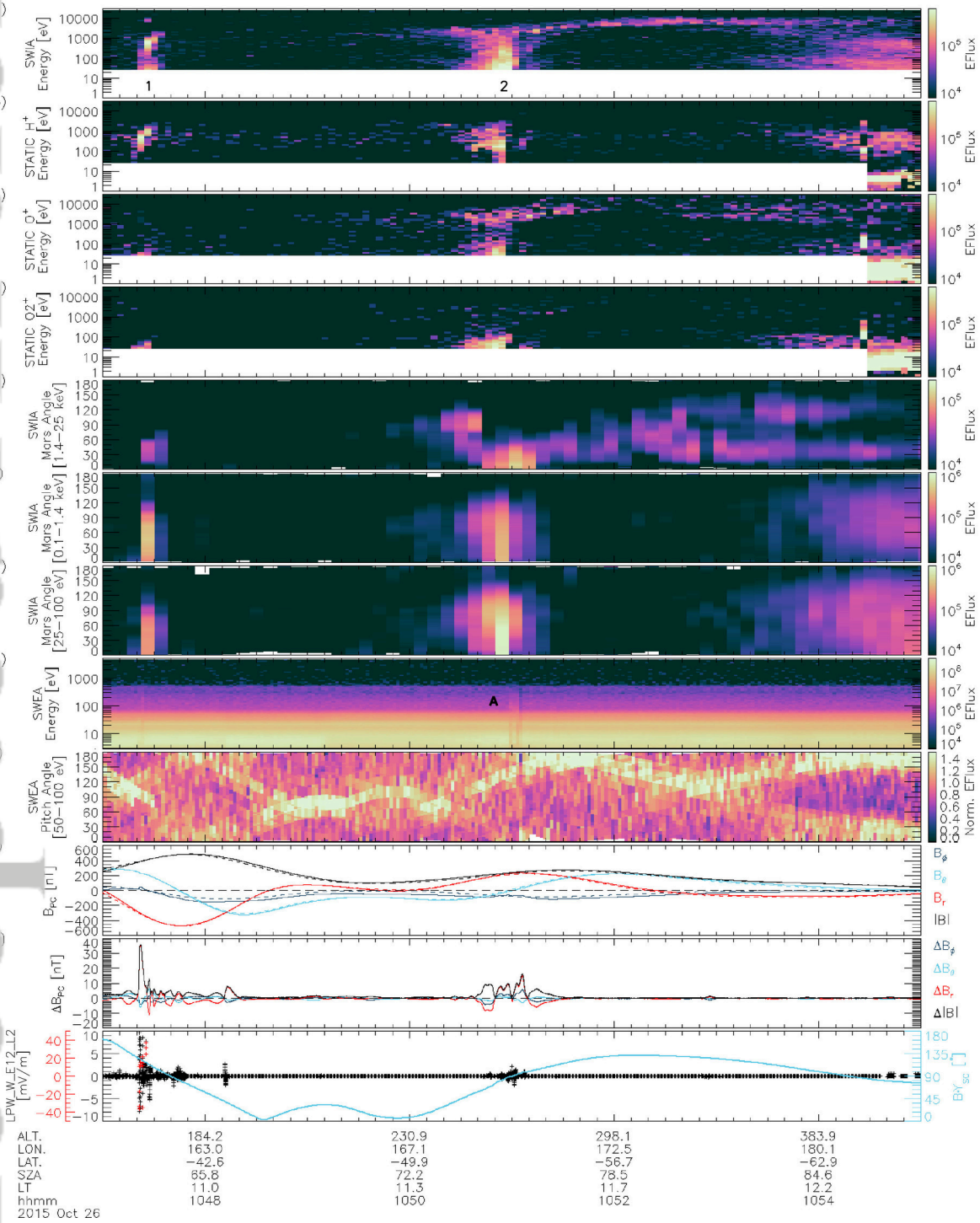

2018ja025569-f01-z-.eps

©2018 American Geophysical Union. All rights reserved.

Accepted Article

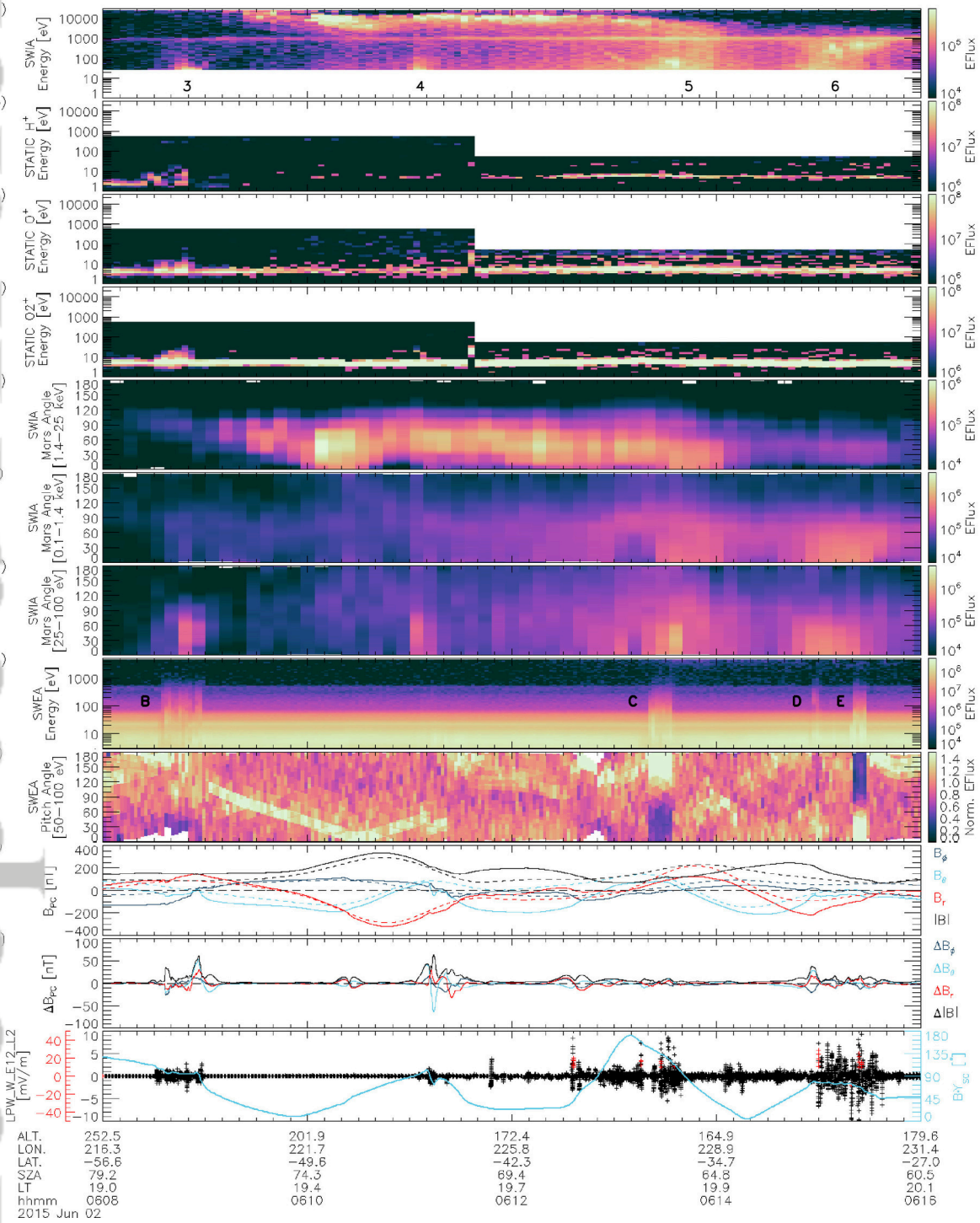

2018ja025569-f02-z-.eps

©2018 American Geophysical Union. All rights reserved.

Accepted Article

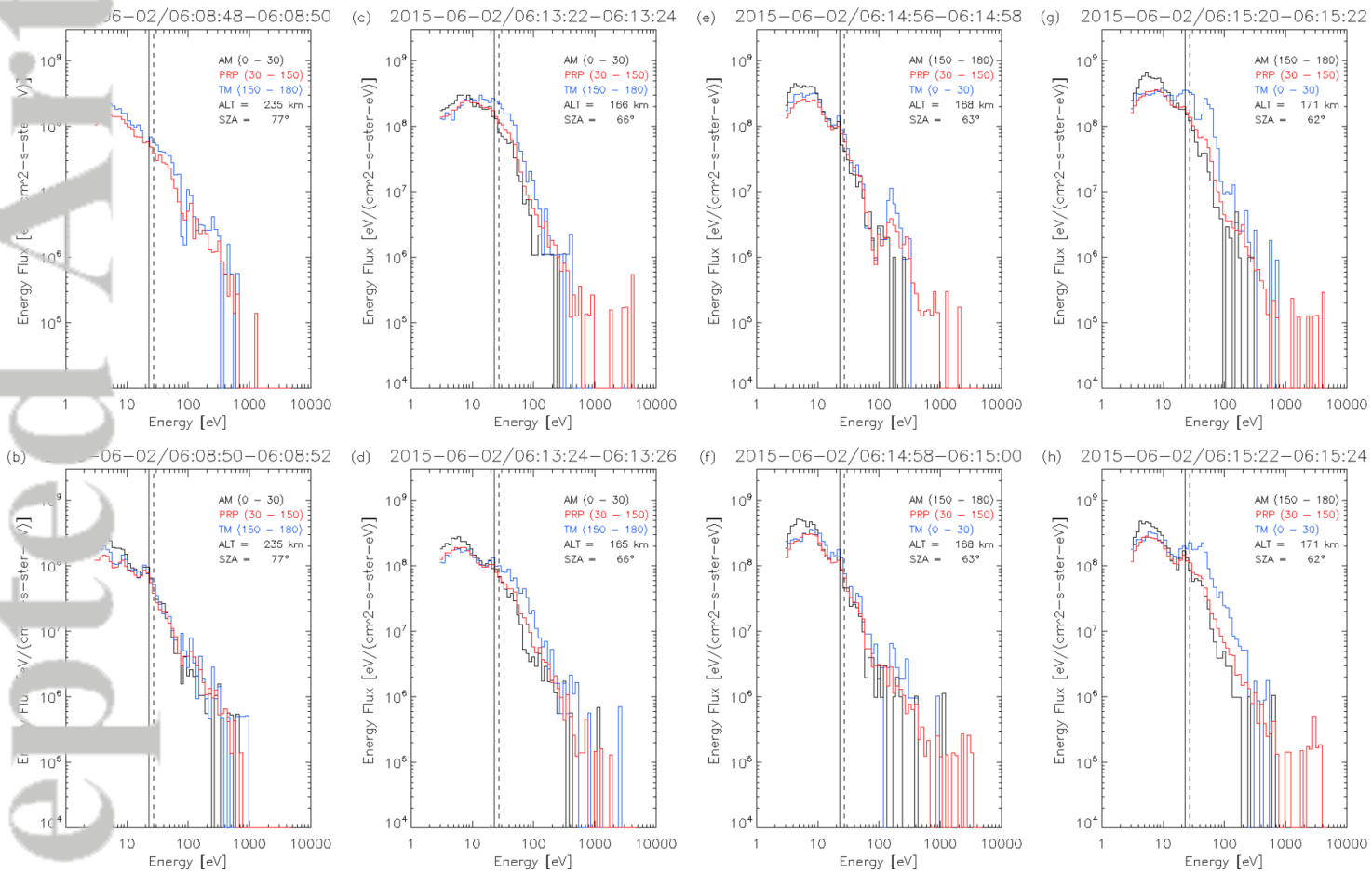

2018JA025569-f03-z-.png

©2018 American Geophysical Union. All rights reserved.

Accepted Article

(a)

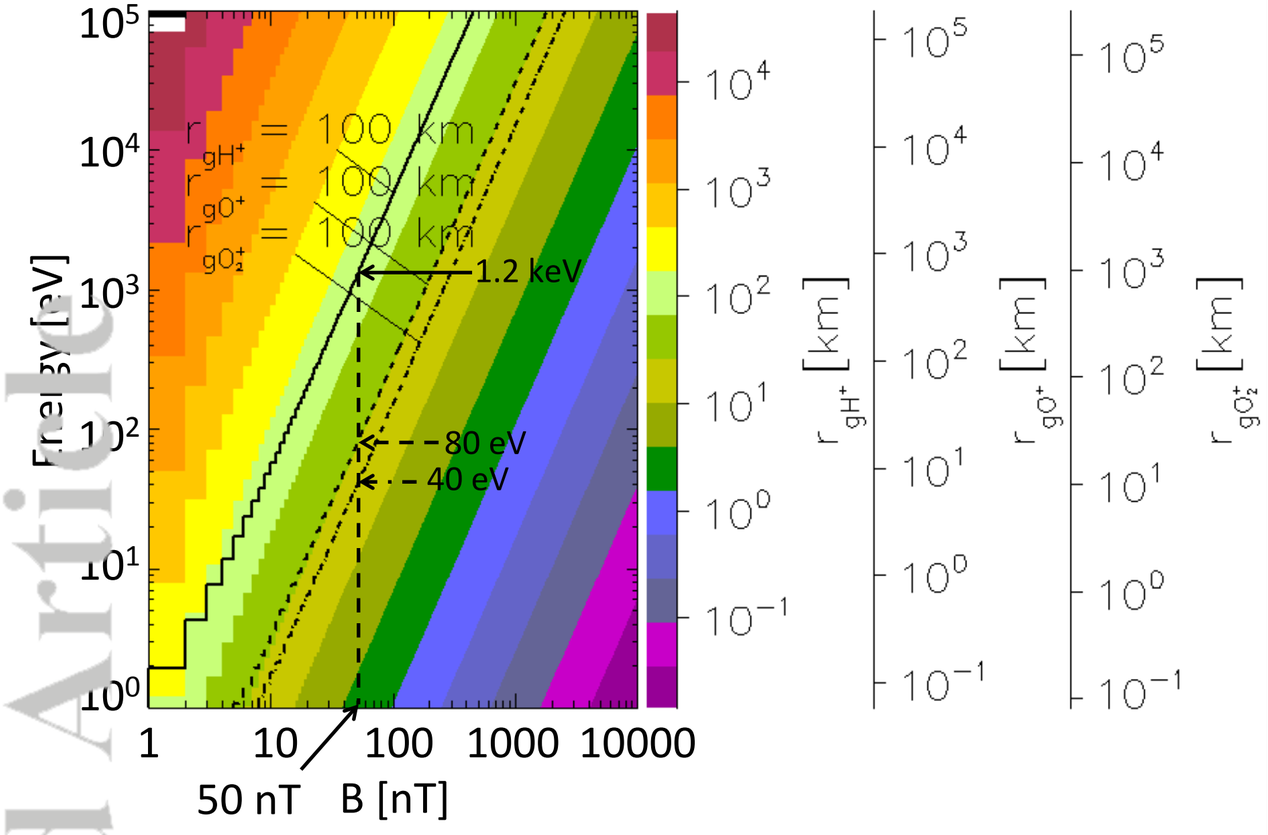

(b) **Scenario 1 - Gyro-forces of less importance, e.g. |B|< 50 nT, H^+ > 100 eV or |B|> 50 nT, O^+ > 1 keV: Injection from surrounding flows - deflection by crustal magnetic fields (not magnetically connected).**

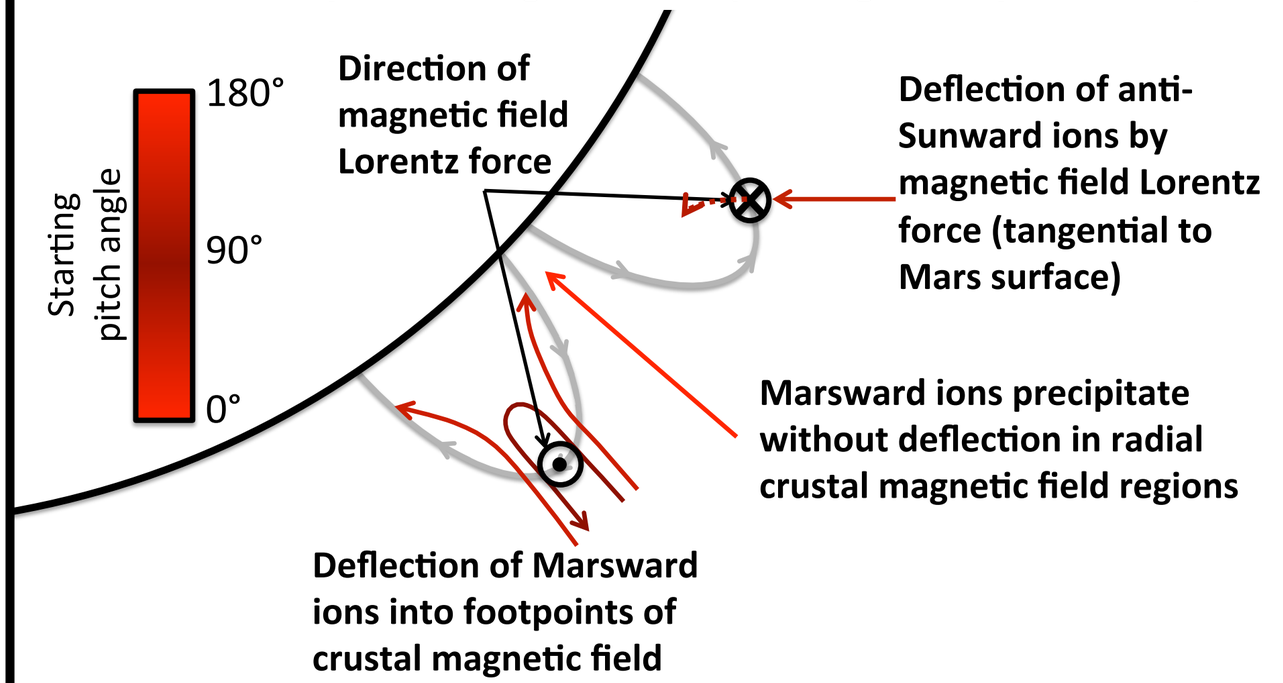

(c) **Scenario 2 - Reconnection and gyro-forces, e.g. |B|> 50 nT, H^+ < 1.2 keV, O^+ < 80 eV and O_2^+ < 40 eV: Injection after magnetic reconnection – flowing ion distributions precipitate and adiabatically mirror (magnetically connected).**

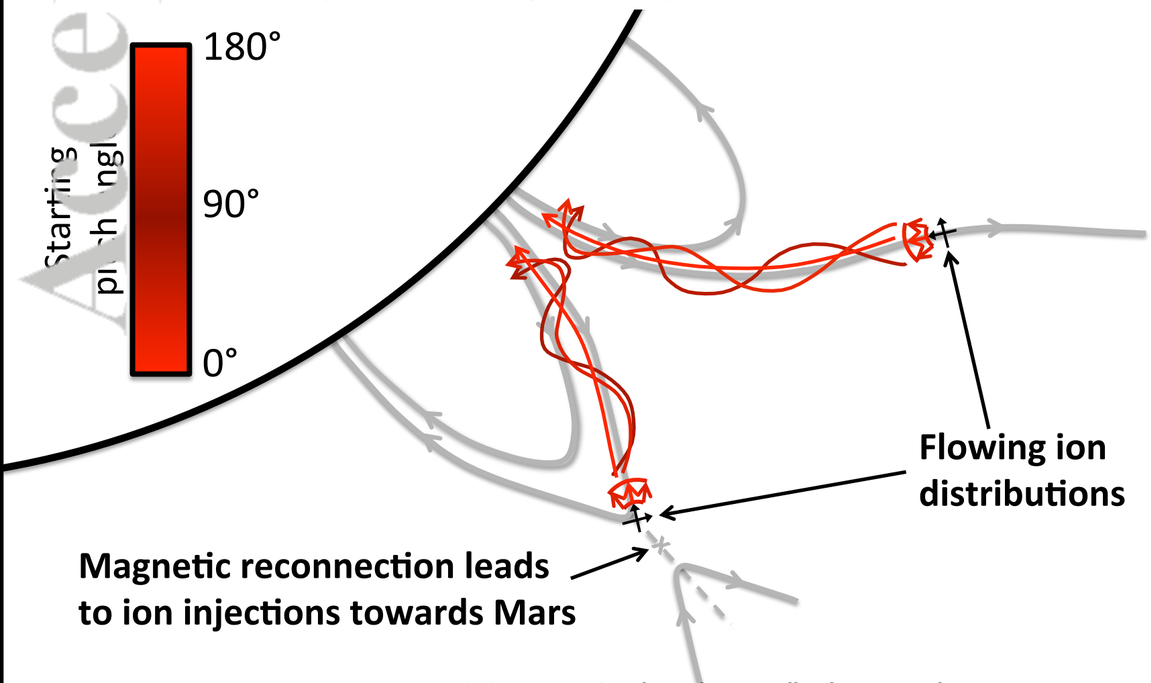

(d) **Scenario 3 - Filling of loss cone and gyro-forces, e.g. |B|> 50 nT and H^+ < 1.2 keV, O^+ < 80 eV and O_2^+ < 40 eV: Pitch angle scattering from non-adiabatic behavior at higher altitude − ions fill loss cone, precipitate and adiabatically mirror (magnetically connected).**

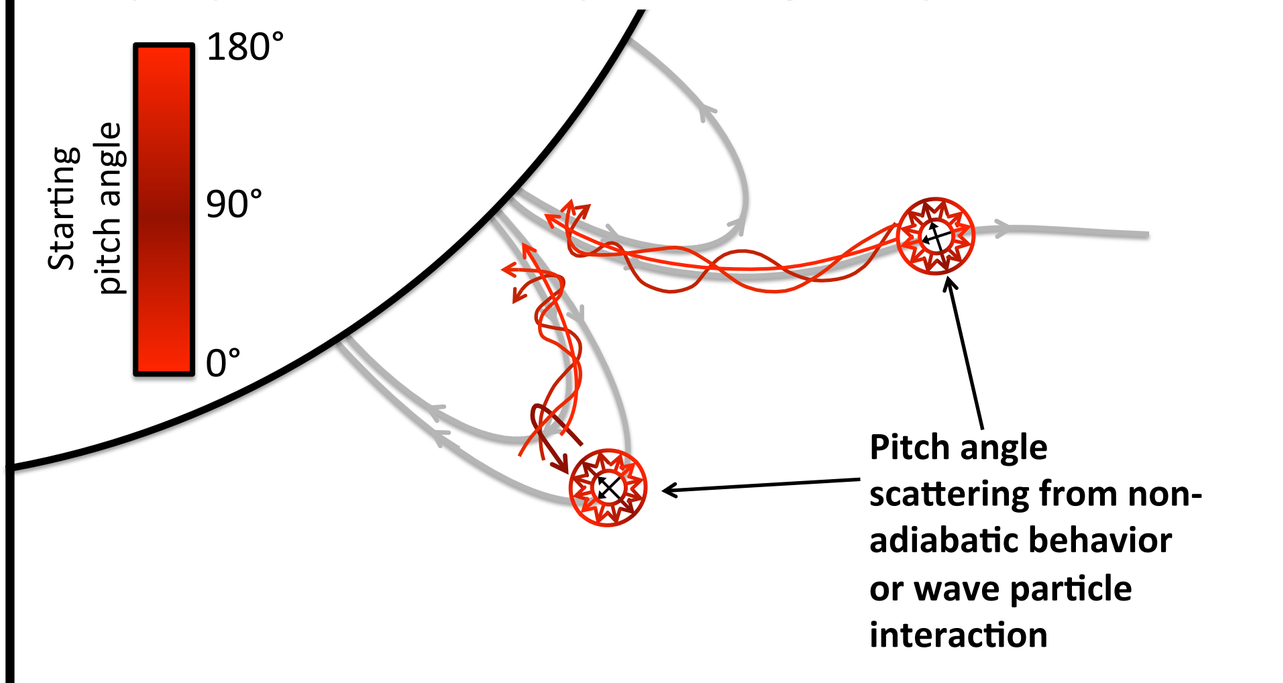

©2018 American Geophysical Union. All rights reserved.

Accepted Article

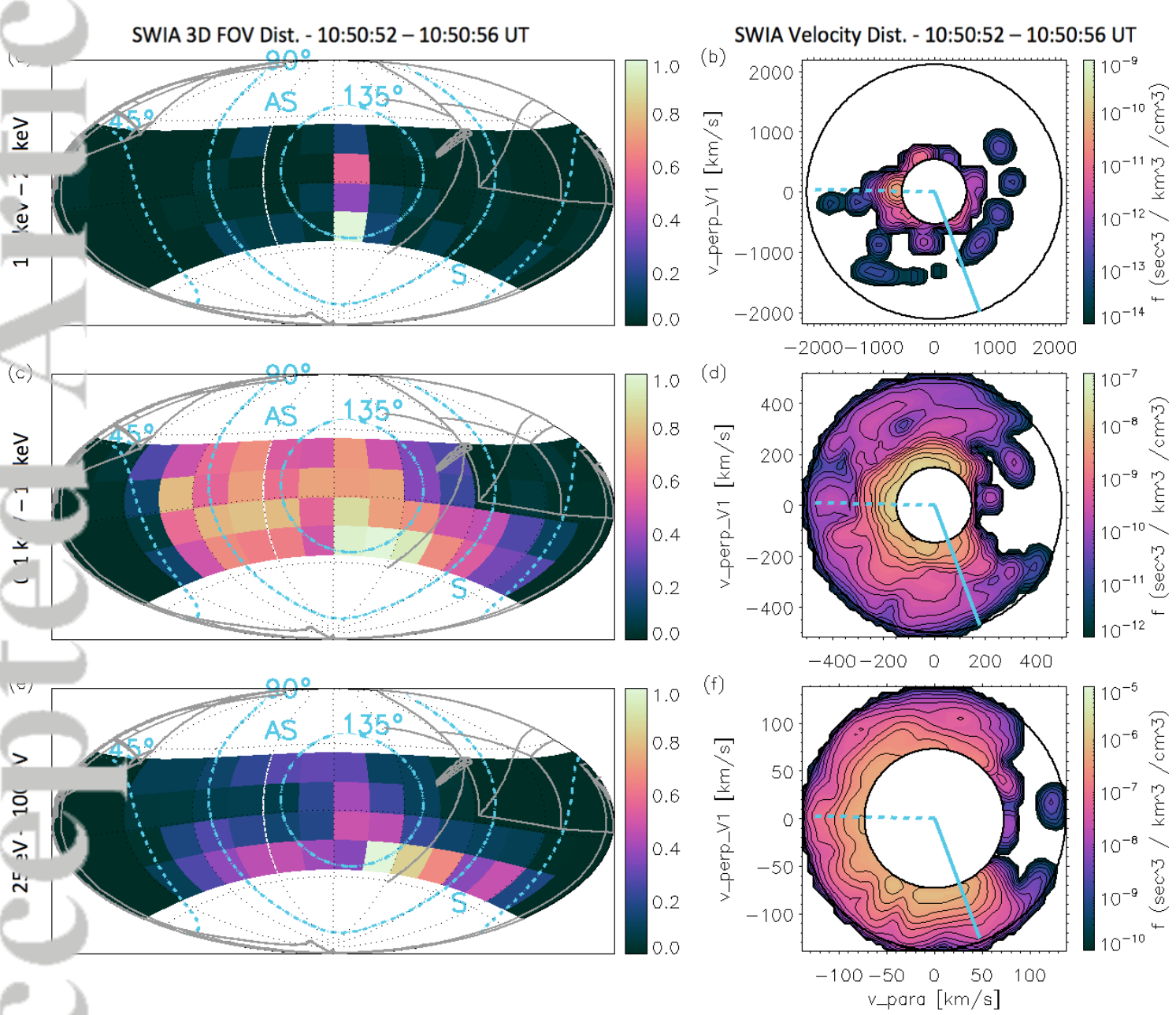

2018JA025569-f05-z-.png

©2018 American Geophysical Union. All rights reserved.

Accepted Article

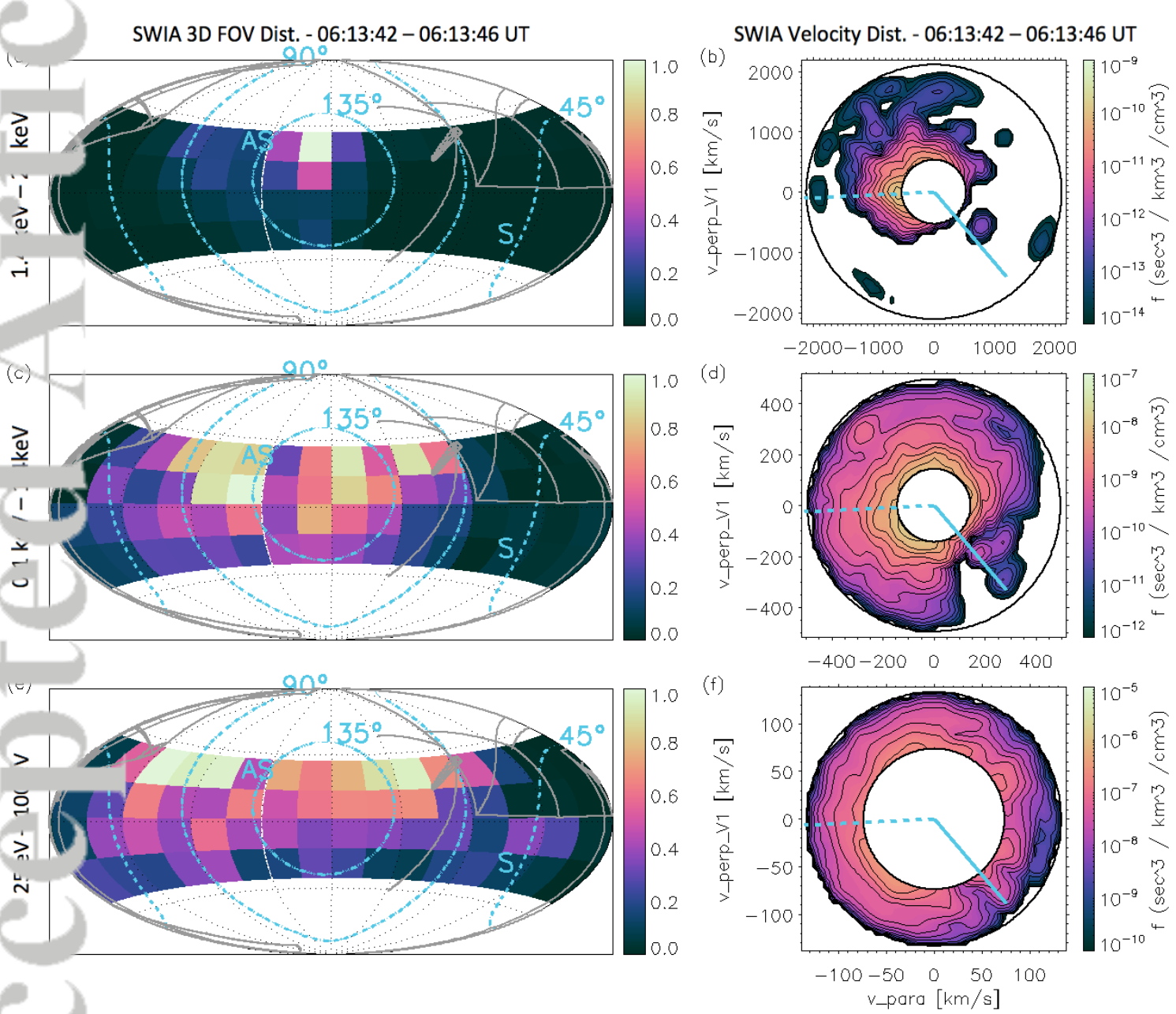

2018JA025569-f06-z-.png

©2018 American Geophysical Union. All rights reserved.

Accepted Article

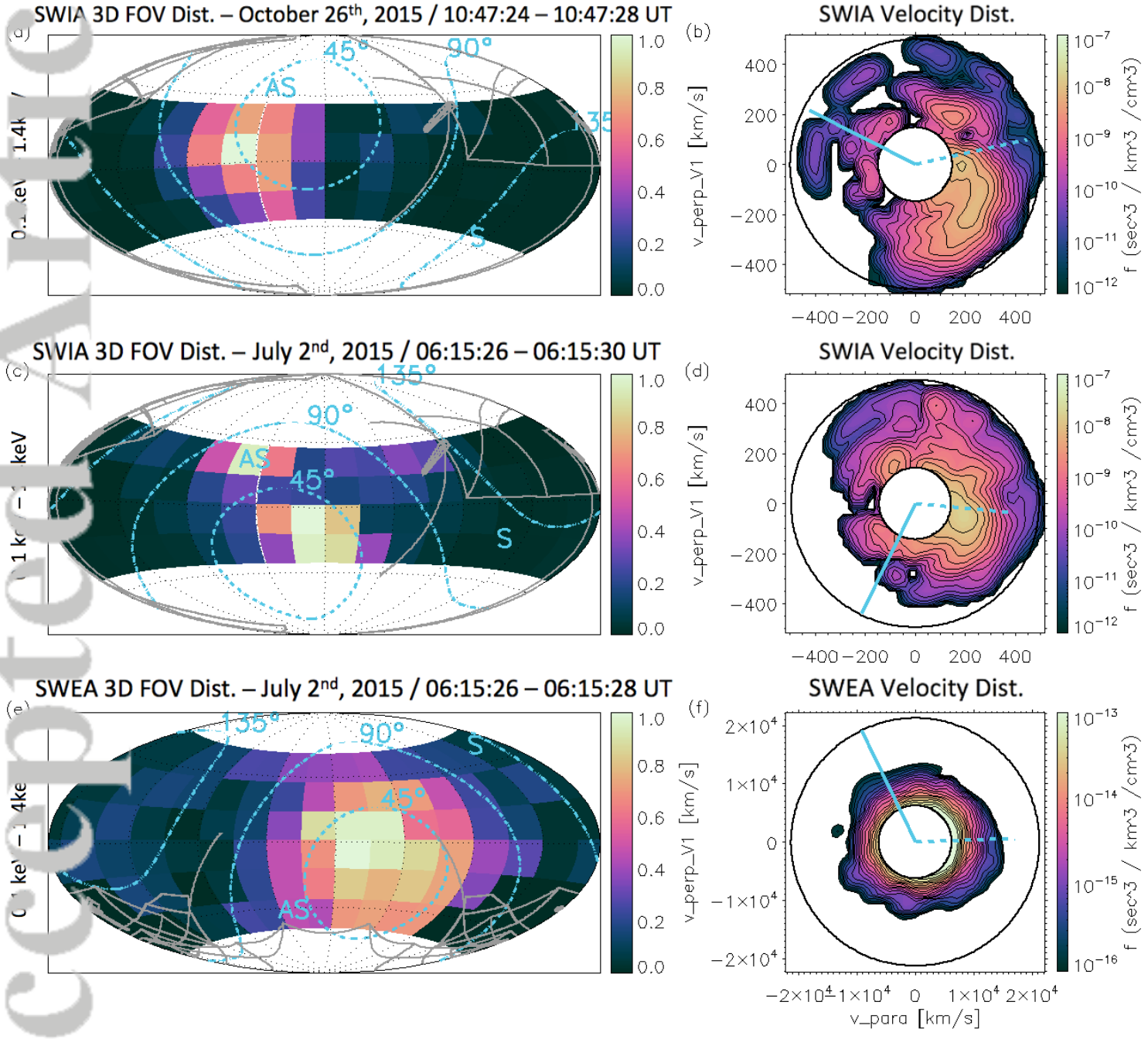

2018JA025569-f07-z-.png

©2018 American Geophysical Union. All rights reserved.

Accepted Article

(a) **Reflected ions and electrons observed at different altitudes:**
Observations of accelerated electrons, magnetic field perturbations and large electric field wave amplitude are all features indicative of a parallel potential drop, possibly due to a charge separation dynamo.

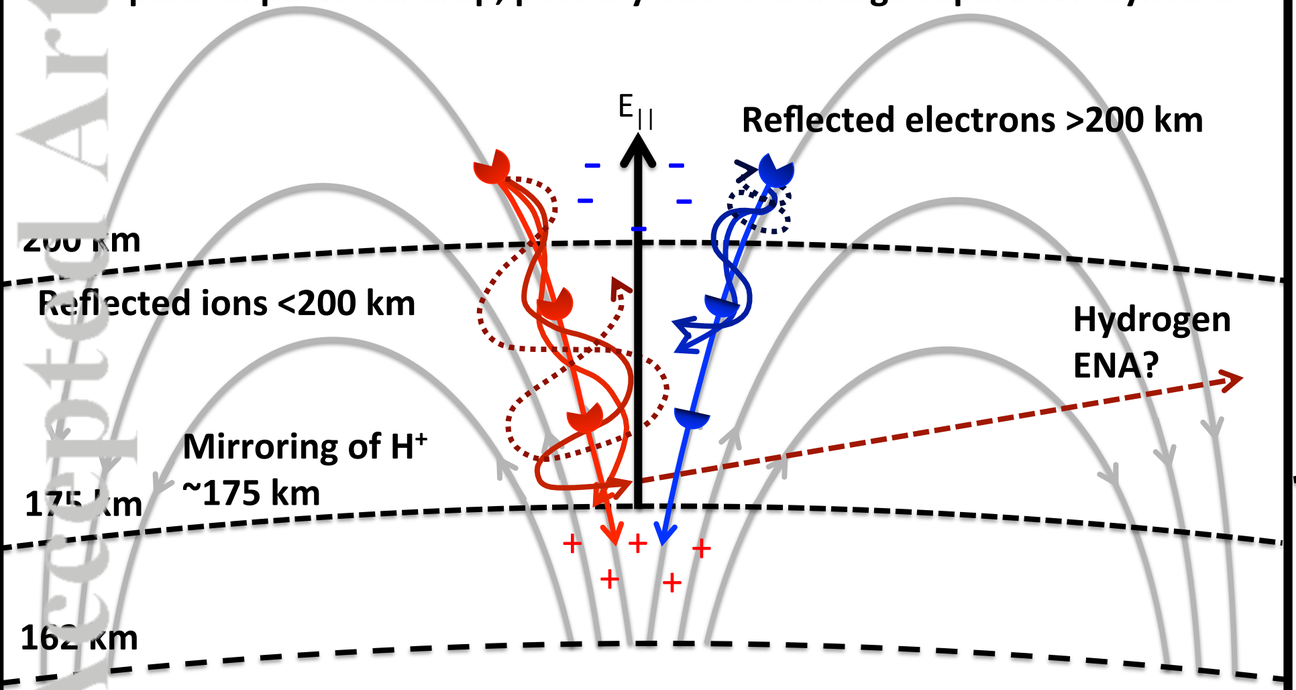

©2018 American Geophysical Union. All rights reserved.

(b) **Crustal magnetic field velocity selection effect on keV O^+ ions:**
O^+ ions picked-up at greater distances have higher energy and more anti-Sunward trajectories at Mars and experience greater reflection at radial magnetic fields.

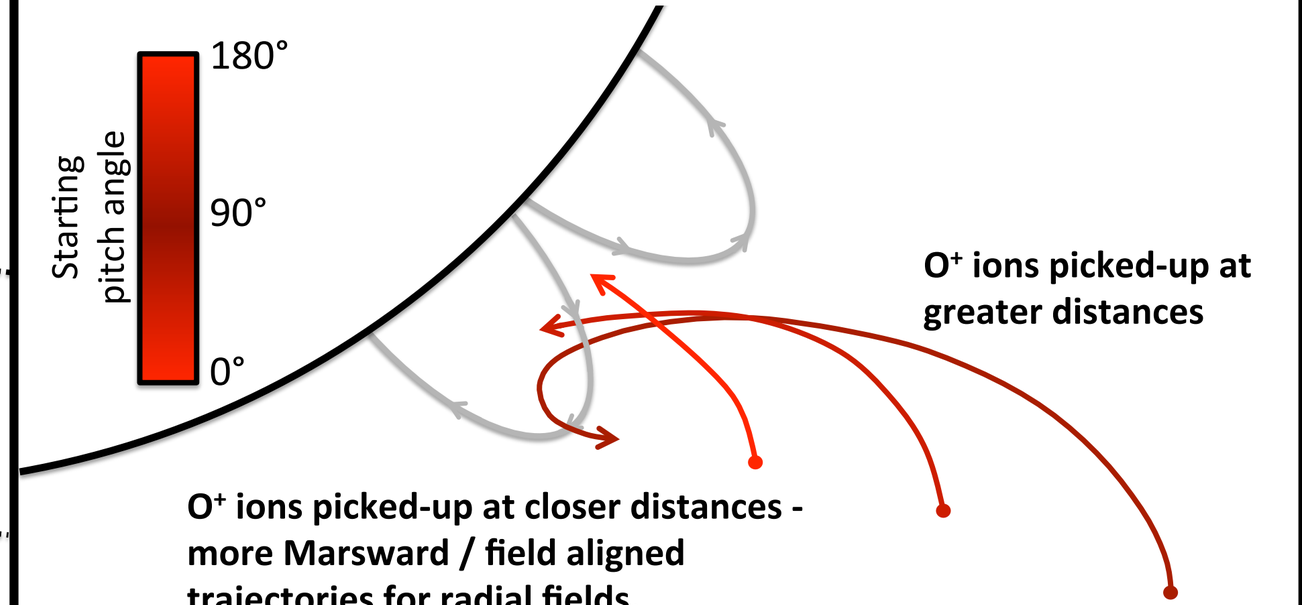

Accepted Article

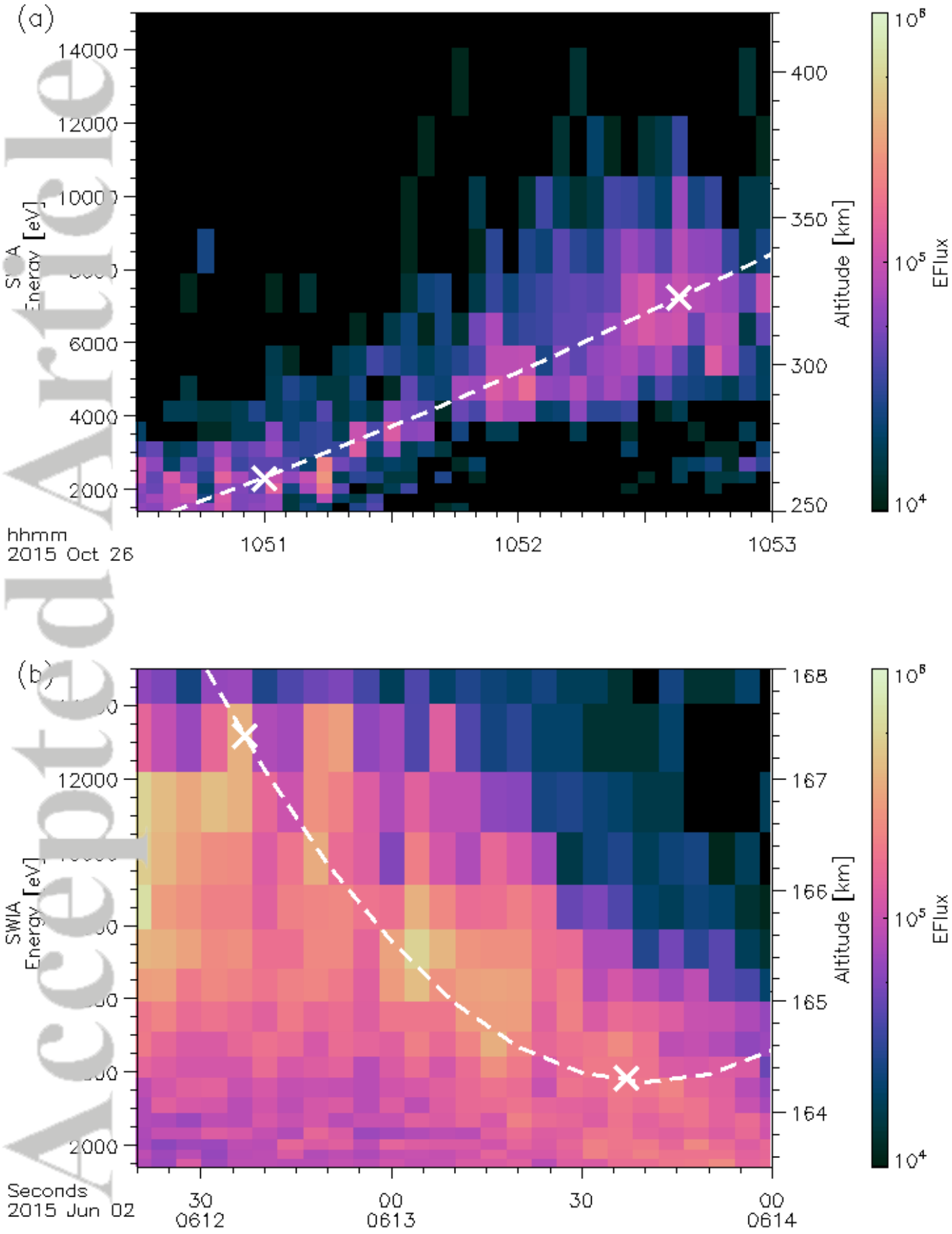

2018JA025569-f09-z-.png

©2018 American Geophysical Union. All rights reserved.